7

Contact Angle and Surface Tension Measurement

KENJI KATOH Osaka City University, Osaka, Japan

I. INTRODUCTION

The wetting phenomenon is an important issue in various technological processes. In some fields, liquids are desired to spread over solid surfaces, e.g., lubrication oils on metallic surfaces or paint on paper. On the other hand, it is necessary for hydrophobic coatings to repel water such as Teflon film on frying pans. The behavior of bubbles on solid surfaces immersed in liquid often has important effects on the performance of industrial apparatus dealing boiling or condensation. In these problems regarding wetting, it is known that the behavior of a drop or bubble on a solid surface is dependent on the three interfacial tensions between solid, gas, and liquid phases, as shown in Fig. 1. The tangential force balance between these interfacial tensions on the three-phase contact line leads to the following well-known Young's equation [1]:

$$\sigma_{SV} - \sigma_{SL} = \sigma_{LV} \cos \alpha_Y. \tag{1}$$

σ_{SV}, σ_{SL}, and σ_{LV} indicate solid–vapor, solid–liquid, and liquid–vapor interfacial tensions, respectively. The environmental atmosphere is assumed to be filled with saturated vapor of liquid. When a drop is exposed to air, however, σ_{LV} usually does not change because a thin layer of saturated vapor may be formed around the drop [2]. In the right-hand side of Eq. (1), α_Y is the angle between the solid surface and the liquid–vapor interface measured from the inside of the liquid phase and is called the contact angle. When the difference between the two interfacial tensions on the left-hand side of Eq. (1) is large enough to make α_Y on the right-hand side small, the solid is favorably wetted by the liquid. As the drop size becomes sufficiently small and the curvature of the solid–gas–liquid contact line becomes quite large, we should add a term representing the effect of line tension to the above equation [3]. In this

Copyright n 2004 by Marcel Dekker, Inc. All Rights Reserved.

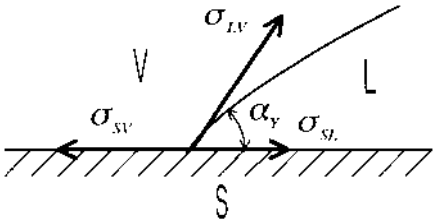

FIG. 1 Force balance on solid–liquid–gas interface.

case, such a term, i.e., line tension times the curvature of the three-phase contact line, appears in the right-hand side of Eq. (1), and the contact angle changes from α_Y to balance with the left-hand side. The line tension might play an important role in the wetting phenomenon in some problems, although this is not yet understood clearly. In this section, we do not touch on the effect of line tension and we use Eq. (1) exclusively. Readers interested in the role of line tension are referred to references [3].

We can regard the interfacial tension represented in Eq. (1) as the free energy per unit area of the interface [4].This may be readily understood by imagining a soap film surrounded by a square wire with one movable side. The liquid–vapor interfacial tension is equal to the work necessary to spread the film surface by a unit area, opposing the tension acting on the movable side [5]. Hence we can regard Eq. (1) as the relation between three kinds of energies, i.e., we can calculate the reversible energy change ($\sigma_{SV}-\sigma_{SL}$) using σ_{LV} cos α_Y without knowledge of σ_{SV} or σ_{SL} themselves when a unit area of the solid surface is wetted by liquid. It is usually not easy to directly measure the interfacial tensions on the left-hand side of Eq. (1), and the wetting behavior is often discussed using σ_{LV} and α_Y.

It is noted that Eq. (1) holds for an ideally smooth and homogeneous solid surface. We cannot write the same relation as Eq. (1) for the contact angle macroscopically observed on a practical solid surface with inhomogeneity such as roughness or heterogeneity due to adsorption. As shown in Fig. 2, different contact angles usually appear, depending on the direction of liquid movement, i.e., the advancing contact angle θ_A is observed when the liquid wets the solid surface, and the receding contact angle θ_R is observed as the solid surface becomes dry upon the retreat of the liquid. This is called the "hysteresis phenomenon of the contact angle." When we put a liquid drop onto a solid surface without any special care, we usually observe a contact angle between the above two extreme values. The hysteresis phenomenon is influenced in a complicated manner by roughness and heterogeneity of the solid surface and also by the irreversible movement of the three-phase contact line. Many authors have extensively investigated the influence of these factors

Copyright n 2004 by Marcel Dekker, Inc. All Rights Reserved.

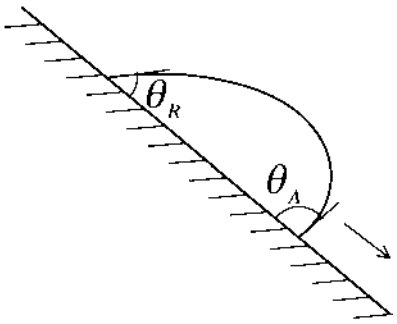

FIG. 2 Contact angle hysteresis observed when a drop rolls down on a slope.

on wetting behavior [6–21]. Although the mechanism of how the macroscopic contact angles are determined is not yet clearly understood, we often use the advancing or receding contact angles as basic quantities indicating the wettability between a liquid and a solid surface. In this section, we call the contact angle defined by Eq. (1) Young's contact angle to distinguish it from the macroscopically observed contact angles θ_A and θ_R.

The correct values of the liquid–vapor interfacial tension and contact angle are necessary to analyze the wetting problems stated at the beginning of this section. Many methods have thus far been proposed for the measurement of these basic quantities. The methods may be classified into two categories, i.e., (1) methods of measuring the dynamic quantities and (2) methods of measuring the geometrical quantities. The Wilhelmy [22] and Du Noüy [23] methods for the measurement of liquid–vapor interfacial tension are typical examples of (1). In these methods, a clean glass plate or ring with zero contact angle is drawn from the liquid and the liquid–vapor interfacial tension acting on the periphery is measured directly using devices such as a microbalance. These methods may also be applied to the measurement of the contact angle by using a test plate, to which the test liquid attaches at certain contact angle, instead of a glass plate [24]. The maximum bubble pressure or drop weight method is another example of (1) for the measurement of interfacial tension [25,26]. Both involve the use of force balance on the bubble or drop due to interfacial tension. The interfacial tension is calculated from the measurement of pressure inside the bubble in the former method and from the drop weight in the latter when it detaches from an orifice. Generally, the Wilhelmy, Du Noüy, and drop weight methods are widely used for the measurement of interfacial tension.

The capillary rise method is a classical example of category (2) for measuring liquid–vapor interfacial tension, in which the liquid height in a capillary tube is measured [27]. On the other hand, the geometrical shape of the

Copyright n 2004 by Marcel Dekker, Inc. All Rights Reserved.

liquid–vapor interface, such as drop or bubble, is often used as the object of measurement. It is well known that the geometry of the interface can be determined by the following Laplace equation [28]:

$$\sigma_{LV}\left(\frac{1}{R_1}+\frac{1}{R_2}\right)=\Delta P, \tag{2}$$

where R_1 and R_2 indicate the principle radii of curvature of the interface and ΔP is the pressure difference between gas and liquid phases. Equation (2) indicates the force balance acting on the liquid–vapor interface and can be solved analytically or numerically. If ΔP, such as the static pressure of liquid due to gravitational force, is known, the interfacial tension can be obtained by measuring the geometric specifications of the interface, such as drop height and radius [29–31]. Contact angles of the drop or bubble are often measured directly using a telescope with a goniometer or in photographs [32]. The tilted plate method is another example of direct measurement of the contact angle, in which a plate immersed in liquid is tilted until the liquid meniscus becomes horizontal at the point of contact [33]. The inclined angle of the plate is equal to the contact angle. The method of using a sessile or pendant drop described above can be applied to the measurement of the contact angle since the geometrical shape is also dependent on the contact angle as a boundary condition on the solid surface [34]. Sometimes the capillary rise of the meniscus attached to a vertical plate is measured to obtain contact angles. The geometry of the meniscus is also determined by Eq. (2), and the contact angle can be easily calculated from the measured height [35].

All the above methods are classic for the measurement of the liquid–vapor interfacial tension and the contact angle and have long been used. Detailed reviews of the measurement of interfacial tension and the contact angle have been given in Refs. [5] and [35–37]. Recently, the above methods have been made more sophisticated and precise by using elaborate techniques such as lasers, computers, and graphic data processing [39–52]. Please refer to those references for details.

Each method mentioned above has its own advantage. However, the methods of category (1) require an accurate apparatus for measuring force because the surface tension is usually small. Similarly, an optical or other device is necessary to measure the geometry of a drop or the liquid meniscus in methods of category (2) since they are not measured directly. Although many sophisticated methods have been considered, the measurements of surface tension and contact angle are generally not so easy and somewhat expensive.

In this section, we discuss a new method for measuring the liquid–vapor interfacial tension and the contact angle based on a principle different from those proposed in the past. One can see a liquid meniscus formed under a solid

Copyright n 2004 by Marcel Dekker, Inc. All Rights Reserved.

such as a needle when it is drawn from a liquid bath. If the solid is raised further, the meniscus spontaneously drops off the surface. This phenomenon might be the result of some kind of thermodynamic or other instability and might be related to the wetting characteristics between the solid and liquid. If the mathematical relationship could be derived theoretically between the critical height of the solid when the meniscus falls off and the wetting, we could obtain the liquid–vapor interfacial tension or contact angle simply by direct measurement of that height. Below, we first discuss the measurement method based on the thermodynamic instability of the liquid meniscus. For the theoretical consideration of instability, a method of calculating the energy due to wetting behavior when hysteresis of contact angle occurs will be proposed. Secondly, we discuss the feasibility of the method based on the geometrical instability of the liquid meniscus.

II. MEASURING METHOD APPLYING THE THERMODYNAMIC INSTABILITY OF LIQUID MENISCUS

A. Hysteresis and Macroscopic Contact Angle

As stated in Section I, advancing and receding contact angles are observed in the macroscopic wetting behavior. There have been many reports regarding the effect of roughness or inhomogeneity on the hysteresis phenomenon of the contact angle. Johnson and Dettre [7,36] considered the thermodynamic free energy of a system consisting of a spherical drop on a solid surface with concentric regular roughness and heterogeneity. The free energy of the system was calculated, varying the attached surface area of a drop of constant volume. There are numerous metastable states corresponding to the local minima of the system energy. Johnson and Dettre explained the hysteresis phenomenon by suggesting that the extreme contact angles among the metastable states appear when the liquid advances or recedes. Later, Eick et al. [8] and Li and Neumann [17] discussed in detail a problem similar to that treated by Johnson and Dettre, but including gravitational energy. The validity of those analyses was verified experimentally, to some extent, for a surface with regular two-dimensional roughness [10,53]. On the other hand, Joanny and de Gennes [12] and Jansons [13] considered the behavior of the three-phase contact line when it moves past a single defect such as a circular hollow or heterogeneous region. They showed that the state of force balance is different between advancement and retreat of the contact line and also discussed the relation of hysteresis to irreversible dissipation occurring when the contact line passes over the defect region. Although those reports presented an interesting concept, the mechanism of hysteresis is not yet understood

Copyright n 2004 by Marcel Dekker, Inc. All Rights Reserved.

completely. For example, Johnson and Dettre et al. discussed the wetting behavior only for the static state, and the results obtained by Joanny and de Gennes et al. are limited to the special case of a single defect. Besides the roughness or heterogeneity stated above, some authors have discussed the effect of line tension on the wetting behavior [3,54–56].

The theoretical considerations mentioned above are based on the assumption that Eq. (1) holds locally on the solid surface, i.e., the inhomogeneous surface is a collection of small homogeneous patches. In this case, the infinitesimal energy change ΔE_W when the liquid wets the solid surface reversibly can be calculated at each local portion as

$$\Delta E_W = -\sigma_{LV} \cos \alpha_Y \Delta s, \tag{3}$$

where Δs indicates the infinitesimal surface area of one homogeneous patch. In Eq. (3), Young's contact angle α_Y is a function of position on the solid surface. Hence it is necessary to integrate Eq. (3) for the calculation of E_W over the entire surface as

$$E_W = -\sigma_{LV} \iint_s \cos \alpha_Y \mathrm{d}s. \tag{4}$$

In the above equation, effects of both the roughness (change of surface area) and heterogeneity (change of α_Y) are included in the integration. It is noted that Eq. (4) holds when the three-phase contact line moves quasi-statically everywhere on the solid surface. We should add extra work if the three-phase contact line moves irreversibly on the solid surface. One can see that the calculation of E_W is complicated and it may be unrealistic to integrate Eq. (4) every time we consider the macroscopic wetting behavior such as mentioned at the beginning of this section.

Wenzel suggested a concept for defining the macroscopic contact angle [57]. He considered a rough surface with constant α_Y. In this case, the energy E_W of Eq. (4) can be written as

$$E_W = -\sigma_{LV} \cos \alpha_Y r S, \tag{5}$$

where r indicates the ratio of the true area of the rough surface to the apparent surface area S. Wenzel's apparent contact angle θ_W is defined as

$$\cos\theta_W = r \cos \alpha_Y, \tag{6}$$

If Wenzel's contact angle actually appears, we can easily calculate the energy change E_W by using measured θ_W as

$$E_W = -\sigma_{LV} \cos \theta_W S \tag{7}$$

We can avoid the difficulty of calculating r by using Eq. (7). In a similar manner, for a smooth but heterogeneous solid surface composed of two

Copyright n 2004 by Marcel Dekker, Inc. All Rights Reserved.

regions with different Young's contact angles α_{Y1} and α_{Y2}, Cassie [58] suggested the following apparent contact angle θ_C:

$$\cos\theta_C = A_1 \cos\alpha_{Y1} + A_2 \cos\alpha_{Y2}, \tag{8}$$

where A_1 and A_2 indicate the proportion of surface area with α_{Y1} and α_{Y2}, respectively. We can also calculate E_W if θ_C is used instead of θ_W in Eq. (7). Although the analysis of the wetting problem can be greatly simplified by the use of θ_W or θ_C, unfortunately, practically observed advancing or receding contact angles are usually different from those angles [17,36]. The reason for this may be considered as follows [11,13]. The definitions of θ_W and θ_C are based on the reversible movement of the three-phase contact line since they are derived from Eq. (3) or Eq. (4). However, irreversible motions inevitably occur at some local positions in the actual wetting behavior. For example, one can observe stick-slip motion when the contact line moves on an inhomogeneous solid surface. Also, extra work might be needed to form a residual drop or gas bubble in a trough of the rough surface when the contact line passes over it. These energies may possibly depend on the direction of contact line movement, i.e., advance and retreat. Some authors consider that these irreversible effects may be the cause of contact angle hysteresis, although the details are not yet clear [11–13]. Wenzel's or Cassie's contact angles do not consider the energies due to irreversibility. Hence we cannot use those angles directly to calculate the actual energy change when the liquid wets the solid surface by some apparent area.

In order to calculate E_W in the macroscopic wetting behavior, here we assume the following rather simple relation:

$$E_W = -\sigma_{LV}\cos\theta S \tag{9}$$

$$\Delta E_W = -\sigma_{LV}\cos\theta \Delta S \tag{10}$$

($\theta = \theta_A$ for advancing and $\theta = \theta_R$ for receding).

Equation (10) is the differential form of Eq. (9). The above equation means that the change of energy when the three-phase contact line advances or recedes on the solid surface by apparent area S can be calculated by using the macroscopically observed contact angles θ_A or θ_R. Equation (9) or Eq. (10) suggests that the effect of irreversible energy change stated above could be wholly reflected by the value of the macroscopic contact angles.

The validity of Eq. (9) or Eq. (10) may be justified by a simple fact. Let us consider a plate with roughness or heterogeneity immersed slowly into a liquid bath, as shown in Fig. 3. A liquid meniscus forms on the plate and its height decreases gradually at the beginning of immersion. When the meniscus height reaches a threshold value, it no longer changes and we can observe the constant contact angle, i.e., advancing angle θ_A. The force $-\sigma_{LV}\cos\theta_A$ acts constantly on the plate during immersion. Since the meniscus shape does not

Copyright n 2004 by Marcel Dekker, Inc. All Rights Reserved.

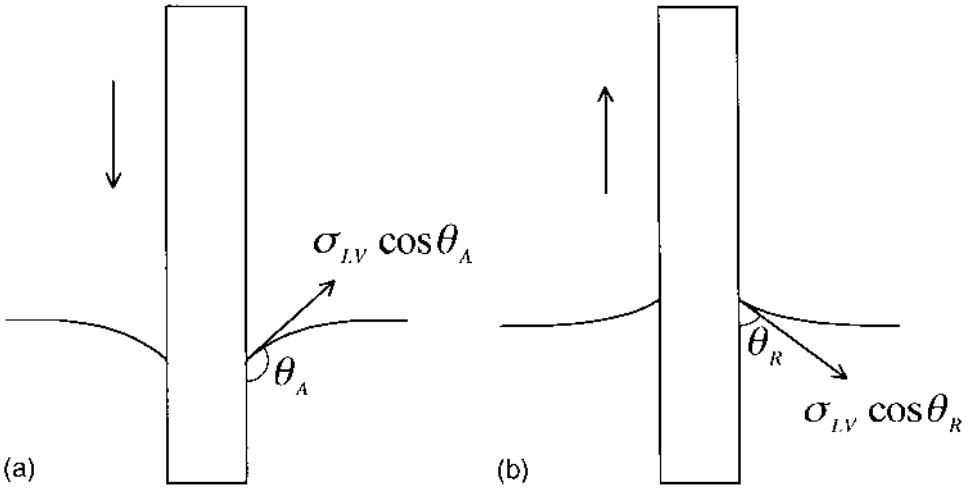

FIG. 3 Liquid–vapor interfacial tension acting on a plate moving quasi-statically: (a) immersion of plate; (b) emersion of plate.

change, the potential energy and the energy related to the liquid–vapor interface area remain constant. Hence the above force would contribute to the work of the liquid wetting the solid plate, i.e., the energy change E_W. In a similar manner, the receding contact angle θ_R can be observed when the plate is slowly drawn from the liquid, and the force $-\sigma_{LV}\cos\theta_R$ produces the energy change E_W. Equations (9) and (10) were verified more rigorously in Ref. [59].

The use of Eq. (9) or Eq. (10) makes it possible to calculate the energy difference E_W from the wetting behavior without touching on the details of the infinitesimal structure of the solid surface or the movement of the three-phase line. In the following, we discuss the instability of the meniscus formed under a solid surface from a thermodynamic viewpoint [60]. The system energy will be estimated based on Eq. (9) or Eq. (10).

B. Wetting Behavior of Two-Dimensional Meniscus Under a Horizontal Plate

One can observe that a meniscus attached to a horizontal plate spontaneously falls off at a certain critical height of the plate. On the other hand, if the plate is immersed into a liquid bath, the liquid spontaneously spreads and wets the entire plate at a critical depth. In this section, we first discuss the unstable phenomenon of a two-dimensional meniscus under a horizontal plate from a thermodynamic viewpoint based on Eq. (10) above. Then, in order to verify

Copyright n 2004 by Marcel Dekker, Inc. All Rights Reserved.

the results, the same problem is considered according to the method in the references [7,8,17,36], in which the infinitesimal effects on the solid surface are taken into consideration.

The energy of the system illustrated in Fig. 4 is calculated when the two-dimensional meniscus attaches to the horizontal plate at macroscopic contact angle θ. S, V, and L in the figure indicate the solid, vapor, and liquid phases, respectively. The coordinates x and z are taken to be the horizontal and vertical directions, respectively. The geometry of the meniscus can be obtained from the solution of Laplace equation (2). The radius of curvature is estimated from differential geometry. Considering the static pressure due to gravitation as ΔP, Eq. (2) is rewritten for the two-dimensional case as [2]

$$\sigma_{\mathrm{LV}} \frac{\dfrac{\mathrm{d}^2 z}{\mathrm{d}x^2}}{\left\{1 + \left(\dfrac{\mathrm{d}z}{\mathrm{d}x}\right)^2\right\}^{3/2}} = \Delta\rho g z, \tag{11}$$

where $\Delta\rho$ and g indicate the difference in density between the liquid and gas phases and the gravitational acceleration, respectively. The nondimensionalized form of Eq. (11) can be written as:

$$\bar{z} = \frac{\mathrm{d}^2\bar{z}/\mathrm{d}\bar{x}^2}{\left\{1 + (\mathrm{d}\bar{z}/\mathrm{d}\bar{x})^2\right\}^{3/2}}. \tag{12}$$

The quantities with an overbar ($\bar{}$) indicate the length nondimensionalized by the following capillary constant:

$$a \equiv \sqrt{\sigma_{\mathrm{LV}}/\Delta\rho g} \tag{13}$$

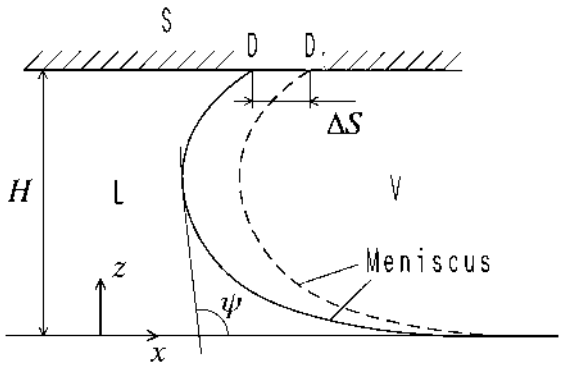

FIG. 4 Two-dimensional meniscus attached to a horizontal plate.

Copyright n 2004 by Marcel Dekker, Inc. All Rights Reserved.

Equation (12) can be solved analytically. Using the inclination angle of the meniscus ψ shown in Fig. 4, the meniscus geometry can be determined by [2]

$$\bar{x} = \left[\ln\left\{ \frac{1 + \sin(\psi/2)}{\cos(\psi/2)} \right\} - 2 \sin \frac{\psi}{2} \right] + C \tag{14}$$

$$\bar{z} = 2 \cos \frac{\psi}{2}, \tag{15}$$

where C is the integral constant.

The infinitesimal energy change is considered when the three-phase contact line shifts by an apparent length ΔS from D to D_1, as seen in Fig. 4. It is noted that ΔS includes roughness or heterogeneity in itself. The contributions to the energy increment are classified into the following three items [8,17]: (1) potential energy of the meniscus ΔE_P, (2) work necessary to increase the liquid–vapor interfacial area ΔE_{LV}, and (3) energy change due to contact line movement ΔE_W. Before the energy of the system in Fig. 4 is discussed, let us calculate energies (1) and (2) for the meniscus attached to an inclined plate, as shown in Fig. 5, for the purpose of generality. Both can be obtained from

$$\Delta E_P = \frac{dE_P}{dS} \Delta S = \frac{d}{dS} \left[\Delta \rho g \left\{ \int_0^H \left(xz - \frac{z^2}{\tan \phi} \right) dz \right\} \right] \Delta S \tag{16}$$

$$\Delta E_P = \frac{dE_{LV}}{dS} \Delta S = \frac{d}{dS} \left[\sigma_{LV} \left\{ \int_0^H \sqrt{1 + (dx/dz)^2}\, dz - \int_0^\infty dx \right\} \right] \Delta S \tag{17}$$

where ϕ and H indicate the angle of plate inclination and the attachment height of the meniscus, as shown in Fig. 5, respectively. E_P and E_{LV} are the potential and liquid–vapor interface energy of the meniscus as a whole, respectively. In the above equations, the horizontal liquid surface is taken as a reference state of energy E_P and E_{LV}. Referring to Li and Neumann [17],

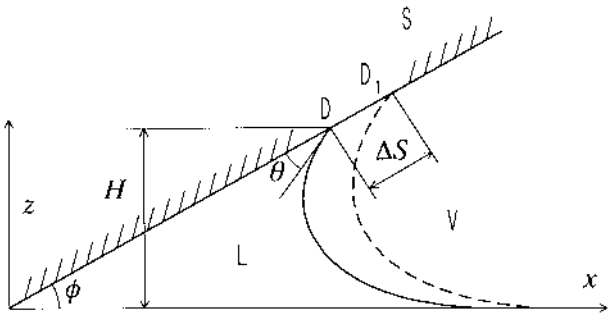

FIG. 5 Two-dimensional meniscus attached to an inclined plate.

Copyright n 2004 by Marcel Dekker, Inc. All Rights Reserved.

the above calculation can be easily obtained by the use of meniscus geometry, i.e., Eqs. (14) and (15). The sum of Eqs. (16) and (17) is written as

$$\Delta E_{\mathrm{P}} + \Delta E_{\mathrm{LV}} = \sigma_{\mathrm{LV}} \cos\theta \Delta S. \tag{18}$$

Equation (18) can also be applied to the meniscus under a horizontal plate shown in Fig. 4. It is noted that in Eq. (18), we neglect the contribution from the liquid in a trough of small roughness with higher order than ΔS. The energy ΔE_{W} is dependent on the direction of contact line movement (i.e., the sign of ΔS), as stated by Eq. (10). The values of ΔE_{W} for liquid advancement and retreat are again written here as

$$\Delta E_{\mathrm{W}} = -\sigma_{\mathrm{LV}} \cos\theta_{\mathrm{A}} \Delta S \quad (\text{advancing}, \Delta S > 0) \tag{19a}$$

$$\Delta E_{\mathrm{W}} = -\sigma_{\mathrm{LV}} \cos\theta_{\mathrm{R}} \Delta S \quad (\text{receding}, \Delta S < 0). \tag{19b}$$

The total energy change of the system,

$$\Delta E = \Delta E_{\mathrm{P}} + \Delta E_{\mathrm{LV}} + \Delta E_{\mathrm{W}}, \tag{20}$$

can be obtained from Eqs. (18), (19a), and (19b), and $(\mathrm{d}E/\mathrm{d}S)$ is written as

$$\frac{\mathrm{d}E}{\mathrm{d}S} = \sigma_{\mathrm{LV}}(\cos\theta - \cos\theta_{\mathrm{A}}) \quad (\text{advancing}) \tag{21a}$$

$$\frac{\mathrm{d}E}{\mathrm{d}S} = \sigma_{\mathrm{LV}}(\cos\theta - \cos\theta_{\mathrm{R}}) \quad (\text{receding}). \tag{21b}$$

Now the behavior of meniscus as shown in Fig. 4 is discussed using Eqs. (21a) and (21b). The meniscus height $\overline{H}$ shown in Fig. 4 is obtained from Eq. (15) as

$$\overline{H} = \sqrt{2(1+\cos\theta)}. \tag{22}$$

First, we discuss the case of meniscus height $\overline{H} < \sqrt{2(1+\cos\theta_{\mathrm{A}})}$, i.e., $\theta > \theta_{\mathrm{A}}$. The following relation can be written for the differential coefficient of energy from Eq. (21a).

$$\frac{\mathrm{d}E}{\mathrm{d}S} < 0 \quad (\text{advancing})$$

The meniscus spreads spontaneously and wets the entire plate since the system energy decreases monotonically in the direction of advance of the contact line ($\Delta S > 0$). In a similar manner, $(\mathrm{d}E/\mathrm{d}S)$ for retreat can be written from Eq. (21b) as

$$\frac{\mathrm{d}E}{\mathrm{d}S} < 0 \quad (\text{receding}).$$

Copyright n 2004 by Marcel Dekker, Inc. All Rights Reserved.

Since the energy increases in the direction of retreat ($\Delta S < 0$), the system is stable for the retreat of the contact line.

Next, the case of $\overline{H} > \sqrt{2(1+\cos\theta_R)}$, i.e., $\theta < \theta_R$, is considered. The following relation can be written for the retreat, from Eq. (21b),

$$\frac{dE}{dS} > 0 \quad \text{(advancing)}$$

$$\frac{dE}{dS} > 0 \quad \text{(receding)}$$

Since the energy decreases in the direction of retreat ($\Delta S < 0$), the contact line retreats spontaneously, and the meniscus finally falls off the plate.

Lastly, let us consider the system behavior when $\overline{H}$ is in the range of $\sqrt{2(1+\cos\theta_A)} < \overline{H} < \sqrt{2(1+\cos\theta_R)}$, i.e., $\theta_A < \theta < \theta_R$. The following inequalities can be derived from Eqs. (23a) and (23b) for the differential coefficient:

$$\frac{dE}{dS} > 0 \quad \text{(advancing)}$$

$$\frac{dE}{dS} < 0 \quad \text{(receding)}$$

The contact line does not move since the energy increases in the directions of both advance and retreat. This means that the two-dimensional meniscus is stable for macroscopic contact angles between θ_A and θ_R.

It was demonstrated in the above discussion that the meniscus begins to move when the contact angle reaches θ_A or θ_R, but does not move for angles between θ_A and θ_R. This behavior is similar to that of a drop on a plate, described in Section I. In the case of a meniscus under a horizontal plate, however, the unstable phenomenon that the meniscus wets the entire surface or falls off occurs at some critical height of the plate corresponding to advancing or receding contact angles. Those phenomena can easily be observed by the naked eye. This suggests the possibility of obtaining the value of macroscopic contact angles by simple measurement of the critical heights. Since the height of a solid surface can be measured directly, we do not need any optical device, unlike the measurement of drop geometry or capillary height of the meniscus.

The above results regarding the system energy can be schematically summarized, as shown in Fig. 6. The figure shows the change of energy E with apparent displacement S for various values of θ. The energy curves in Fig. 6 are drawn straight according to the following relation:

$$\frac{d^2E}{dS^2} = -\sigma_{LV}\sin\theta\frac{d\theta}{dS} = 0. \tag{23}$$

Copyright n 2004 by Marcel Dekker, Inc. All Rights Reserved.

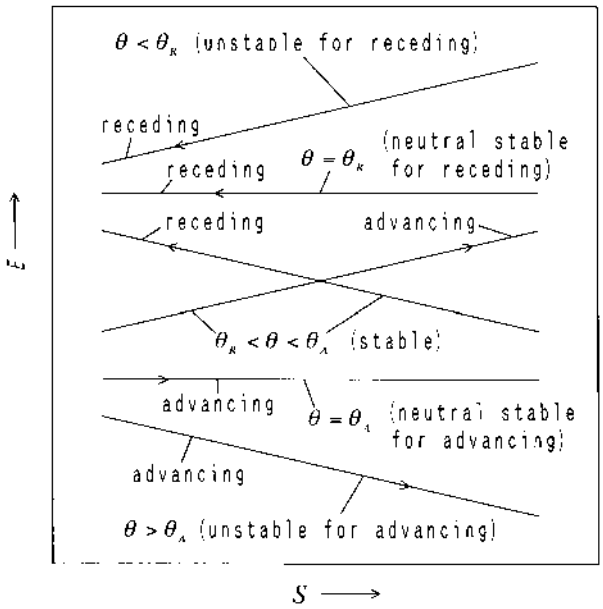

FIG. 6 Schematic of system energy change with the shift of attachment position of meniscus on a horizontal plate: the system becomes unstable when the energy monotonically decreases in the direction of the shift.

The above equation can be derived by the differentiation of Eq. (21) and $(d\theta/dS) = 0$ (the shape of a two-dimensional meniscus does not change with S, as seen in Fig. 4). As shown in Fig. 6, the system becomes neutral stable when $\theta = \theta_A$ or $\theta = \theta_R$.

The above discussion is based on Eq. (9) or Eq. (10) in which the infinitesimal effects on the solid surface are assumed to be wholly reflected by the macroscopic contact angles θ_A and θ_R. The use of Eqs. (9) and (10) makes it simple to analyze the macroscopic wetting behavior of a two-dimensional meniscus under a horizontal plate. In order to confirm the validity of the analysis using Eqs. (9) and (10), the same problem is discussed using the method in which the effect of roughness is taken into consideration. As stated before, there have been many reports concerning the wetting behavior on a rough surface. Unfortunately, the movement of the contact line on a surface with random roughness is not yet understood completely. Here we choose the relatively simple model for two-dimensional roughness treated by Eick et al. [8]. As shown in Fig. 7, we discuss the two-dimensional meniscus under a horizontal plate with a saw-tooth cross section. The surface is made up of a

Copyright n 2004 by Marcel Dekker, Inc. All Rights Reserved.

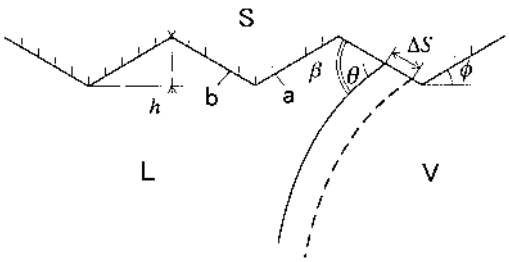

FIG. 7 Two-dimensional meniscus attached to a horizontal plate with small saw-tooth roughness: microscopic view of Fig. 4.

repetition of two small alternation slopes with the same inclination ϕ to the horizontal axis. Young's contact angle α_Y is assumed to be constant over the entire surface. As shown in the figure, h and β indicate the roughness height and the angle between the meniscus and the solid surface from a microscopic viewpoint, respectively. θ is the macroscopically observed contact angle as stated before. The change of system energy is considered when the contact line shifts by Δs on the inclined side of roughness, where Δs represents the infinitesimal distance along the side and is different from the apparent ΔS used in Eqs. (10), (19a), and (19b). The work necessary to change the potential energy and the liquid–vapor interfacial area of the meniscus can be calculated, for the inclined plate, from Eq. (18) as

$$\Delta E_P + \Delta E_{LV} = \sigma_{LV} \cos \beta \Delta s. \tag{24}$$

The energy change ΔE_W due to the movement of the three-phase contact line should be derived using Eq. (3), in this case, as

$$\Delta E_W = -\sigma_{LV} \cos \alpha_Y \Delta s. \tag{25}$$

From Eqs. (24) and (25), the rate of energy change is written as

$$\frac{dE}{ds} = \sigma_{LV}(\cos \beta - \cos \alpha_Y). \tag{26}$$

The above equation must be considered separately for side a and side b shown in Fig. 7. The following relations are obtained for α and β if we substitute the relations $\beta = \theta - \phi$ for α and $\beta = \theta + \phi$ for β into Eq. (26).

$$\left(\frac{dE}{ds}\right)_a = \sigma_{LV}\{\cos(\theta - \phi) - \cos \alpha_Y\} \tag{27}$$

$$\left(\frac{dE}{ds}\right)_b = \sigma_{LV}\{\cos(\theta + \phi) - \cos \alpha_Y\} \tag{28}$$

Copyright n 2004 by Marcel Dekker, Inc. All Rights Reserved.

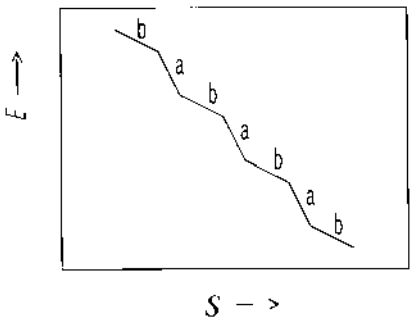

FIG. 8 System energy change with the shift of the meniscus shown in Fig. 7: in the case of $\overline{H} < \sqrt{2\{1+\cos(\alpha_Y+\phi)\}}$, at which the system is unstable in the advance direction.

First, let us consider the case of apparent contact angle $\theta > \alpha_Y + \phi$ [i.e., the meniscus height $\overline{H} < \sqrt{2\{1+\cos(\alpha_Y+\phi)\}}$ from Eq. (22)]. The following inequality holds, from Eqs. (27) and (28):

$$\left(\frac{dE}{ds}\right)_b < \left(\frac{dE}{ds}\right)_a < 0. \tag{29}$$

The energy curve can be depicted as shown in Fig. 8 based on the above relation. As is clear in the figure, the energy decreases monotonically for the movement in the positive direction of s. Hence the meniscus spreads and wets the entire plate spontaneously. The system becomes neutral stable at $\theta = \alpha_Y + \phi$, as shown in Fig. 9.

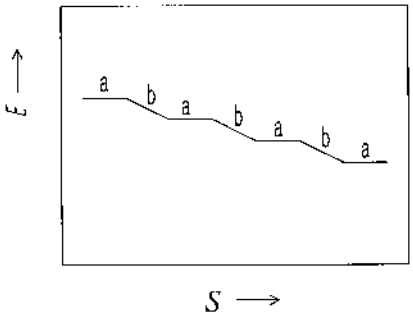

FIG. 9 System energy change with the shift of the meniscus in the case of $\overline{H} = \sqrt{2\{1+\cos(\alpha_Y+\phi)\}}$, at which the system is neutral stable in the advance direction.

Copyright n 2004 by Marcel Dekker, Inc. All Rights Reserved.

Next, when $\theta < \alpha_Y - \phi$ (i.e., $\overline{H} > \sqrt{2\{1+\cos(\alpha_Y - \phi)\}}$), the following relation can be derived for the differential coefficient of E in a similar manner as Eq. (29).

$$\left(\frac{dE}{ds}\right)_a > \left(\frac{dE}{ds}\right)_b > 0. \tag{30}$$

According to the above relation, the energy curve can be schematically shown as that in Fig. 10. As seen in the figure, the meniscus is unstable in the receding direction of the contact line and falls off the plate. When $\theta = \alpha_Y + \phi$, the system is at neutral stability, as in Fig. 9.

Finally, when $\alpha_Y - \phi < \theta < \alpha_Y + \phi$ (i.e., $\sqrt{2\{1+\cos(\alpha_Y + \phi)\}} < \overline{H} < \sqrt{2\{1+\cos(\alpha_Y - \phi)\}}$), the following inequality holds:

$$\left(\frac{dE}{ds}\right)_a > 0, \quad \left(\frac{dE}{ds}\right)_b < 0. \tag{31}$$

Fig. 11 shows the energy curve obtained according to Eq. (31). The energy exhibits a local minimum at the vertex of the roughness between a and b shown in Fig. 7. The system is stable because there are many positions with minimum energy.

Eick et al. [8] analyzed the wetting behavior of a two-dimensional meniscus attached to a vertical plate with roughness similar to that depicted in Fig. 7. They suggested the following relations for the macroscopically observed contact angles.

$$\theta_A = \alpha_Y + \phi \tag{32a}$$

$$\theta_R = \alpha_Y - \phi \tag{32b}$$

Using Eqs. (32a) and (32b), the above results from Eqs. (29)–(31) can be summarized in Table 1. If Eqs. (32a) and (32b) are valid for the macroscopic

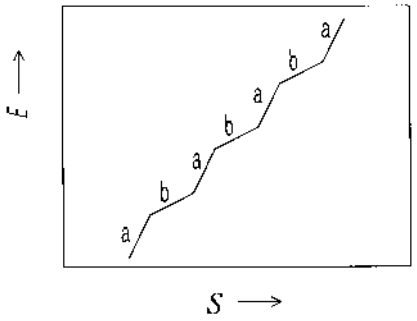

FIG. 10 System energy change with the shift of the meniscus in the case of $\overline{H} > \sqrt{2\{1+\cos(\alpha_Y - \phi)\}}$, at which the system is unstable in the retreat direction.

Copyright n 2004 by Marcel Dekker, Inc. All Rights Reserved.

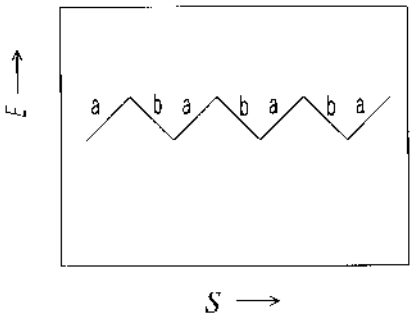

FIG. 11 System energy change with the shift of the meniscus in the case of $\sqrt{2\{1+\cos(\alpha_Y+\phi)\}} < \overline{H} < \sqrt{2\{1+\cos(\alpha_Y-\phi)\}}$ at which the system is stable.

contact angles, the results given in Table 1 are the same as those shown in Fig. 6 derived based on Eq. (10). Similar results can be obtained for a smooth plate with two-dimensional heterogeneity of regular shape [60]. Hence it seems to be possible to analyze the macroscopic wetting behavior based on the assumption of Eq. (9) or Eq. (10). The roughness or heterogeneity assumed here is quite simple. The analysis would be more difficult for a general surface with random characteristics if the infinitesimal effects were taken into consideration. It is evident that the method of using Eqs. (9) and (10) is quite simple compared with the above method.

C. Unstable Behavior of Axisymmetric Meniscus

It seems possible to measure contact angles by applying the thermodynamic instability of a two-dimensional meniscus, as stated above. However, there are many metastable positions on the horizontal plate as shown in Fig. 11,

TABLE 1 Wetting Behavior of Two-Dimensional Meniscus Under a Horizontal Plate: The Behavior is Analyzed from a Microscopic Viewpoint

θ	$\overline{H}$	Advance of meniscus	Retreat of meniscus
$\theta > \theta_A$	$\overline{H} < \sqrt{2(1+\cos\theta_A)}$	Unstable	Stable
$\theta = \theta_A$	$\overline{H} = \sqrt{2(1+\cos\theta_A)}$	Neutral stable	Stable
$\theta_R < \theta_A < \theta_A$	$\sqrt{2(1+\cos\theta_A)} < \overline{H} < \sqrt{2(1+\cos\theta_R)}$	Stable	Stable
$\theta = \theta_R$	$\overline{H} = \sqrt{2(1+\cos\theta_R)}$	Stable	Neutral stable
$\theta < \theta_R$	$\overline{H} > \sqrt{2(1+\cos\theta_R)}$	Stable	Unstable

Copyright n 2004 by Marcel Dekker, Inc. All Rights Reserved.

which might make the recognition of instability difficult because the attachment point of the meniscus could move among them even under a stable condition. Also, it is actually not very easy to handle the two-dimensional meniscus under a horizontal plate because an axisymmetric meniscus is usually formed when the plate is drawn from a liquid bath. This may be because the axisymmetric shape has less energy than a two-dimensional one.

In this section, let us consider the macroscopic wetting behavior of an axisymmetric meniscus from a thermodynamic viewpoint and discuss the possibility of the measurement of the contact angle and interfacial tension [61]. As in the analysis stated above, the theoretical consideration is based on the assumption described by Eq. (9).

The axisymmetric meniscus under a conical surface is chosen as the subject, as shown in Fig. 12. The cylindrical coordinates r and z are taken to be the radial and horizontal directions, respectively. If some relations of differential geometry are inserted into the radii of curvature in Laplace equation (2), the profile of the axisymmetric meniscus can be determined by the following differential equation [31,62].

$$r\frac{d^2r}{dz^2} - \left(\frac{dr}{dz}\right)^2 - 1 - \frac{1}{\sigma_{LV}}\Delta\rho g r z\left\{1 + \left(\frac{dr}{dz}\right)^2\right\}^{3/2} = 0 \tag{33}$$

The above equation is nondimensionalized by the use of capillary constant a defined by Eq. (13).

$$\bar{r}\frac{d^2\bar{r}}{d\bar{z}^2} - \left(\frac{d\bar{r}}{d\bar{z}}\right)^2 - 1 - \bar{r}\,\bar{z}\left\{1 + \left(\frac{d\bar{r}}{d\bar{z}}\right)^2\right\}^{3/2} = 0 \tag{34}$$

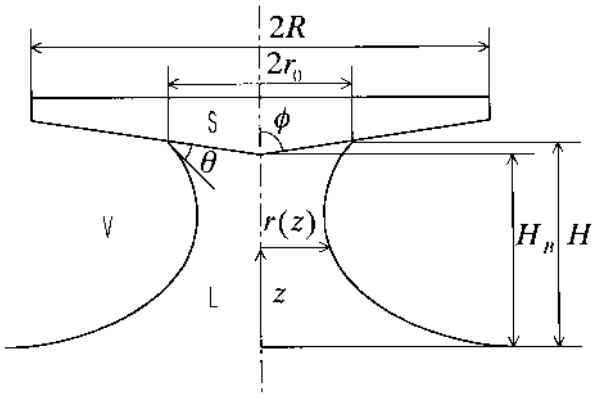

FIG. 12 Schematic of axisymmetric meniscus attached to a downward cone surface.

Copyright n 2004 by Marcel Dekker, Inc. All Rights Reserved.

where $\bar{r} \equiv r/a$ and $\bar{z} \equiv z/a$. The boundary conditions of the meniscus profile shown in Fig. 12 can be written as

$$\bar{z} \to 0: \quad \frac{d\bar{r}}{d\bar{z}} \to -\infty \tag{35}$$

$$\bar{z} = \overline{H}: \quad \bar{r} = \bar{r}_0, \tag{36}$$

where $\overline{H} \equiv H/a$ and $\bar{r}_0 \equiv r_0/a$ indicate the height and radius of the meniscus at the cone surface. In the following, quantities of length are all nondimensionalized by a. Eqs. (34)–(36) were solved numerically [63,64]. Fig. 13 shows a comparison of the meniscus profile calculated numerically with that measured from a photograph. As seen in the figure, the calculated results agree well with the measured profile.

The system energy of Fig. 12 can be estimated by using the above solution for the meniscus profile. As stated in the previous section, we consider the potential energy E_P, the energy of the liquid–vapor interfacial area E_{LV}, and the work done by the three-phase contact line wetting the cone surface E_W. The dry cone surface and the horizontal liquid surface ($z = 0$) are taken for the reference state of system energy. E_P and E_{LV}, which represent the work necessary to form the axisymmetric meniscus shown in Fig. 12, are calculated from

$$E_P = \Delta\rho g\left\{\int_0^H \pi r^2 z\,dz - \int_{H_B}^H \pi(z - H_B)^2 \tan^2\phi\, z\,dz\right\} \tag{37}$$

$$E_{LV} = \sigma_{LV}\left[\int_0^H 2\pi r\left\{\sqrt{1 + \left(\frac{dr}{dz}\right)^2} - \frac{dr}{dz}\right\}dz - \pi r_0^2\right], \tag{38}$$

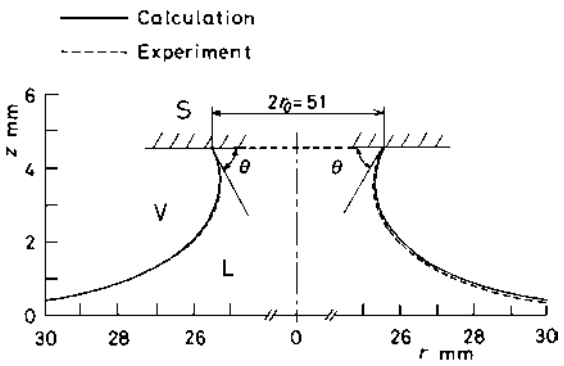

FIG. 13 Comparison of axisymmetric meniscus profile obtained numerically with that measured from a photograph.

Copyright n 2004 by Marcel Dekker, Inc. All Rights Reserved.

where ϕ and H_B indicate the half-vertical angle of the cone and the height of the cone vertex, respectively. Using Eq. (9), the energy change E_W, when the three-phase contact line advances and wets the cone surface to the radius r_0, can be calculated as

$$E_W = -\sigma_{LV}\frac{\pi r_0^2}{\sin\phi}\cos\theta_A \quad \text{(advancing)} \tag{39a}$$

In order to calculate E_W in the receding direction, we should consider that, first, the dry cone surface is completely wetted and then dries to r_0. The energy change during this process can be obtained as

$$E_W = \sigma_{LV}\frac{\pi(R^2 - r_0^2)}{\sin\phi}\cos\theta_R - \sigma_{LV}\frac{\pi R^2}{\sin\phi}\cos\theta_A \quad \text{(receding)}$$

where R is the cone radius shown in Fig. 12. However, it is troublesome to treat the constant quantities in the above equation every time because we are mainly interested in the energy change from one state to another, i.e., the displacement of the meniscus radius r_0. Hence we omit the constant terms in the above equation and write the following expression:

$$E_W = -\sigma_{LV}\frac{\pi r_0^2}{\sin\phi}\cos\theta_R \quad \text{(receding)}, \tag{39b}$$

Equations (37)–(39a,b) are nondimensionalized using the parameter $(\sigma_{LV}{}^2/\Delta\rho g)$.

$$\overline{E}_P = \int_0^{\overline{H}} \pi \bar{r}^2\,\bar{z}\,d\bar{z} - \int_{\overline{H}_B}^{\overline{H}} \pi(\bar{z} - \overline{H}_B)^2 \tan^2\phi\,\bar{z}\,d\bar{z} \tag{40}$$

$$\overline{E}_{LV} = \int_0^{\overline{H}} 2\pi\bar{r}\left\{\sqrt{1 + \left(\frac{d\bar{r}}{d\bar{z}}\right)^2} - \frac{d\bar{r}}{d\bar{z}}\right\}d\bar{z} - \pi\bar{r}_0^2 \tag{41}$$

$$\overline{E}_W = -\frac{\pi\bar{r}_0^2}{\sin\phi}\cos\theta_A \quad \text{(advancing)} \tag{42a}$$

$$\overline{E}_W = -\frac{\pi\bar{r}_0^2}{\sin\phi}\cos\theta_R \quad \text{(receding)} \tag{42b}$$

The overbar, such as $\overline{E}_P$, means nondimensional energy. The total energy of the system is calculated by summing the above equations.

$$\overline{E} = \overline{E}_P + \overline{E}_{LV} + \overline{E}_W \tag{43}$$

Copyright n 2004 by Marcel Dekker, Inc. All Rights Reserved.

First, let us discuss the axisymmetric meniscus attached to a vertical circular cylinder, i.e., $\phi = 0°$. For the cylinder, the energy $\overline{E}_W$ is calculated by the following equation instead of Eqs. (42a) and (42b).

$$\overline{E}_W = -2\pi\bar{r}_0\overline{H}\cos\theta_A \quad \text{(for advancing)} \tag{44a}$$

$$\overline{E}_W = -2\pi\bar{r}_0\overline{H}\cos\theta_R \quad \text{(for receding)} \tag{44b}$$

Fig. 14a and b shows the calculated energy change with the meniscus height $\overline{H}$ and with the apparent contact angle θ for the advancement and the retreat of the three-phase contact line. The nondimensional cylinder radius $\overline{R} = 14.7$ in the figure corresponds to $R = 40$ mm for water of 25°C. Two energy curves are depicted in each figure corresponding to advancing and receding, for which $\theta_A = 60°$ and $\theta_R = 40°$ are assumed in the calculation of $\overline{E}_W$. As shown in Fig. 14a, the system exhibits a minimum energy at $\theta = \theta_A$ or $\theta = \theta_R$ for both curves. This result is similar to that obtained conventional two-dimensional meniscus attached to a smooth and homogeneous plate [8,17], although here we used the macroscopic apparent contact angles for the calculation of $\overline{E}_W$.

Referring to the results of Fig. 14, let us consider the wetting behavior when the cylinder is immersed into a liquid bath in state A shown in Fig. 14, i.e., the energy minimum at $\theta = 40°$. Since the contact line advances on the cylinder

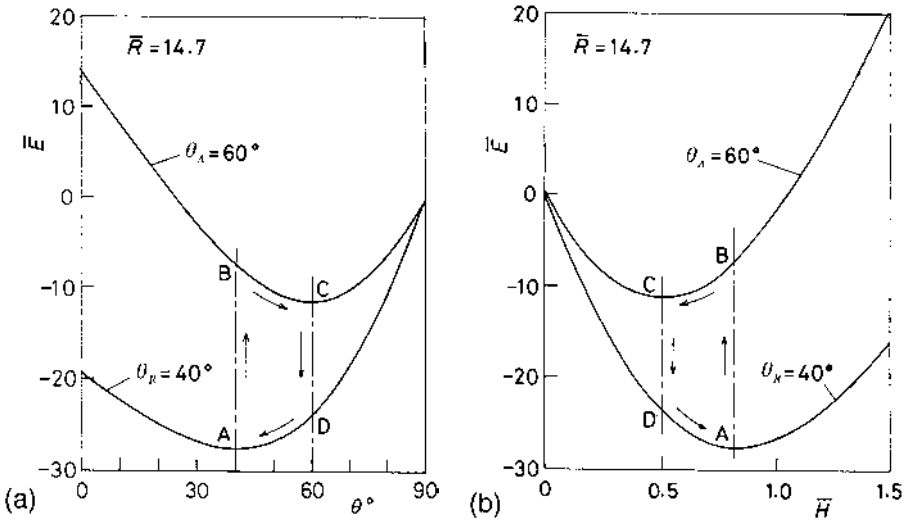

FIG. 14 System energy change with (a) the apparent contact angle θ and (b) nondimensional meniscus height $\overline{H}$, when axisymmetric meniscus attaches to a circular cylinder. The system is stable at states C and A for advance and retreat of meniscus, respectively.

Copyright n 2004 by Marcel Dekker, Inc. All Rights Reserved.

surface, we start from state B on the curve of $\theta_A = 60°$. The meniscus height $\overline{H}$ decreases with the immersion of the cylinder from B because of the reduction of energy from B to C, as seen in Fig. 14b. Once the system reaches C, at which energy is minimum, $\overline{H}$ no longer decreases and is constant. A similar consideration holds for the retreat of the contact line. Inversely, when the cylinder is raised from C, we start at D on the curve $\theta_R = 40°$. Once the system reaches A, $\overline{H}$ remains constant corresponding to $\theta = 40°$. These results are the same as those shown in Fig. 3 in Section I and indicate the general wetting behavior of a meniscus attached to a plate or cylinder observed macroscopically. Here we can explain the mechanism by using the energy curves for advancement and retreat, which were calculated based on the assumption of Eq. (9) that the effects of infinitesimal roughness are entirely reflected in the values of macroscopic contact angles.

Next, the wetting behavior is discussed for an axisymmetric meniscus under a horizontal plate. The calculated results of Eq. (43) for $\phi = 90°$ are shown in Fig. 15 for the plate height $\overline{H} = 1.62$. We assume that $\theta_A = 60°$ and $\theta_R = 40°$, similar to Fig. 14. The abscissa $\bar{r}_0$ in Fig. 15b is the meniscus radius of attachment to the plate. As shown in Fig. 15a, the energy exhibits a maximum value at each contact angle, contrary to the results shown in Fig. 14. These results are quite different from the general understanding that the system is stable when a liquid attaches to a solid surface at an intrinsic contact angle [17]. One would expect that the axisymmetric meniscus under the horizontal plate is unstable and it falls off or wets the entire surface spontaneously. This is not true in practice, and we can explain the observed wetting behavior of the meniscus by using the energy curves in Fig. 15 based on the assumption proposed for the estimation of $\overline{E}_W$. We consider the system behavior in the state between the two maxima A and B shown in Fig. 15. As seen in the figure, since the system energy increases in the directions of both advance and retreat, the meniscus radius $\bar{r}_0$ does not spread or shrink spontaneously, i.e., the system is stable between A and B. On the other hand, when the system is beyond the region between A and B, the contact line moves spontaneously; for example, when the system is on the right side of B, the meniscus wets the entire surface because of the monotonic reduction of energy in the advancement direction, as is clear from the energy curve for $\theta_A = 60°$ shown in Fig. 15b.

If the plate height $\overline{H}$ is decreased from $\overline{H} = 1.62$ of Fig. 15 at the state between A and B, the apparent contact angle θ increases while $\bar{r}_0$ remains constant. The energy curve in Fig. 15b changes its profile during the reduction of height $\overline{H}$, i.e., state B at which energy is maximum gradually shifts to the left, while the positions A and B in Fig. 15a remain unchanged. Finally, the system coincides with state B when θ reaches θ_A at a certain critical height of the plate corresponding to the assumed radius $\bar{r}_0$ between A and B at $\overline{H} = 1.62$. At that time, the system becomes unstable in the direction of advance and the

Copyright n 2004 by Marcel Dekker, Inc. All Rights Reserved.

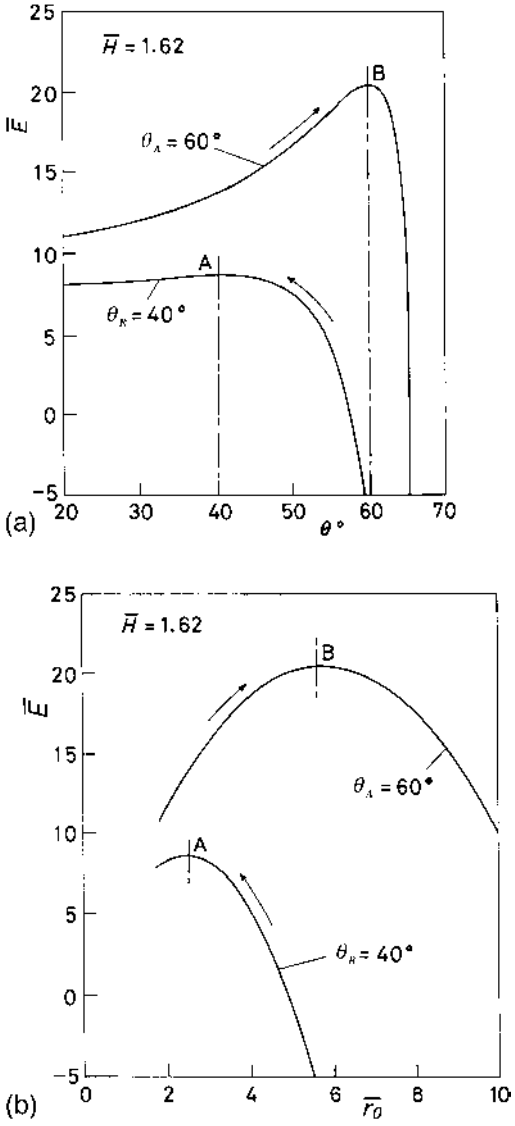

FIG. 15 System energy change with (a) the apparent contact angle θ and (b) nondimensional meniscus radius $\bar{r}_o$, when axisymmetric meniscus forms under a horizontal plate. The system is stable between states A and B.

Copyright n 2004 by Marcel Dekker, Inc. All Rights Reserved.

liquid spontaneously wets the entire plate surface. In a similar manner, when the plate is raised, θ reaches θ_R at a certain critical height. The meniscus becomes unstable for the retreat and falls off the plate surface. These predictions based on the energy curve describe the actual wetting behavior well. The unstable phenomenon occurs at a certain critical height of the plate, as in the case of the two-dimensional meniscus mentioned in Section II.B. This critical height, however, depends not only on the contact angle, but also on the meniscus radius $\bar{r}_0$. Hence it should be necessary to measure the radius in addition to the plate height if we apply the principle to the measurement of contact angles. The measurement of the meniscus radius is not very easy compared with that of the critical height, which makes this method unattractive.

Lastly, let us consider the meniscus attached to a cone surface. Fig. 16 shows the calculated results of the system energy for a cone surface of half-vertex angle $\phi = 60°$. As seen from Fig. 16a, the system exhibits both a minimum and a maximum at each contact angle. It is recognized that the cone surface has characteristics intermediate between those of a cylinder and a plate. The system is stable at the radius $\bar{r}_0$ corresponding to the minimum energy shown in Fig. 16b. Fig. 17 shows the energy curves for various heights

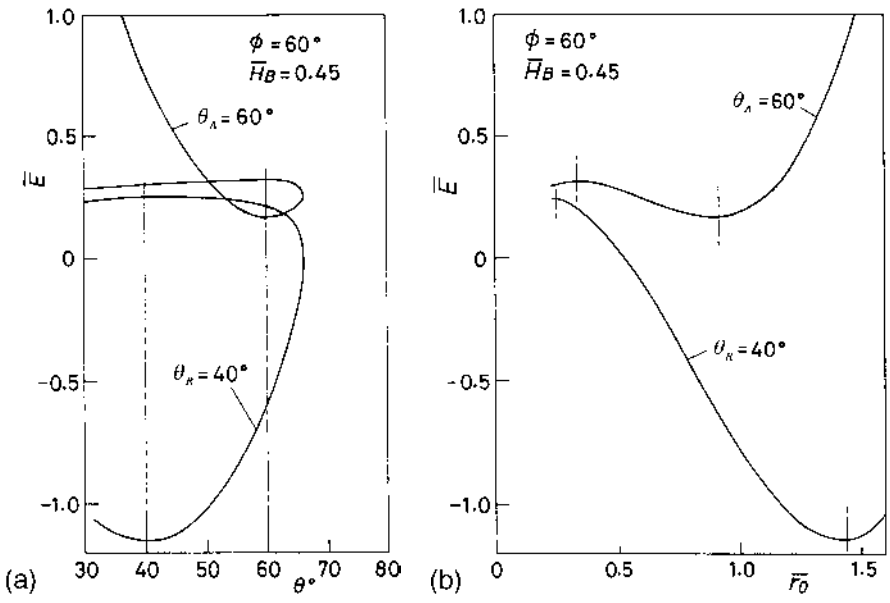

FIG. 16 System energy change with (a) apparent contact angle θ and (b) nondimensional meniscus radius $\bar{r}_o$, when axisymmetric meniscus attaches to a downward cone surface. The system energy exhibits both a minimum and a maximum at advancing and receding contact angles.

Copyright n 2004 by Marcel Dekker, Inc. All Rights Reserved.

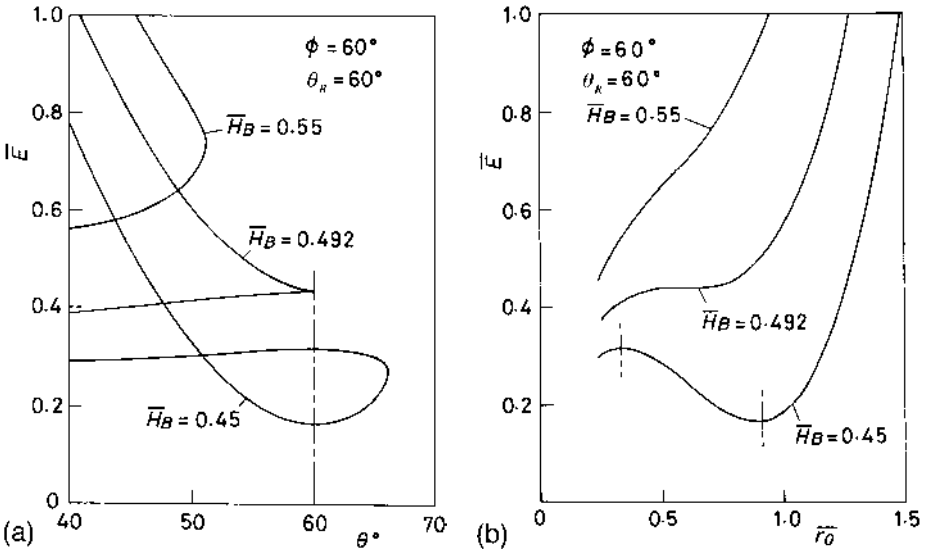

FIG. 17 Energy curve for various cone heights $\bar{H}_B$ shown in Fig. 12. The system does not have energy minimum and becomes unstable in the direction of retreat of meniscus when $\bar{H}_B$ is larger than 0.492.

of the cone vertex $\bar{H}_B$. Here we assume the receding contact angle $\theta_R = 60°$. When the height is relatively low, i.e., $\bar{H}_B = 0.45$, the system energy becomes maximum and minimum at the apparent contact angle $\theta = 60°$, as shown in Fig. 17a. Fig. 17b indicates that when the cone height is raised to $\bar{H}_B = 0.492$, the extreme states disappear from the energy curve and the energy monotonically increases with $\bar{r}_0$. Hence the system becomes unstable in the direction of retreat and the meniscus falls off the cone for $\bar{H}_B$ higher than 0.492. The critical height is dependent only on the receding contact angle θ_R unlike the case of the horizontal plate described above. Moreover, the meniscus radius $\bar{r}_0$ is fixed to that of minimum energy under a stable condition such as $\bar{H}_B = 0.45$ in Fig. 17b, which is different from the two-dimensional meniscus under a horizontal plate where there are many metastable positions on the plate surface. This could make it easy to recognize when instability occurs. It may be possible to obtain θ_R from the measured critical height of $\bar{H}_B$.

A similar result can be obtained for the axisymmetric meniscus attached to an upward cone, as shown in Fig. 18. The coordinate z is taken to be the downward direction, while the other variables are the same as in Fig. 12. $\bar{H}_B$ indicates the depth of the cone vertex. The system energy, instead of $\bar{E}_W$, can be calculated in the same manner as for the downward cone. Here we consider the advance of the three-phase contact line. If we take the dry surface as a

Copyright n 2004 by Marcel Dekker, Inc. All Rights Reserved.

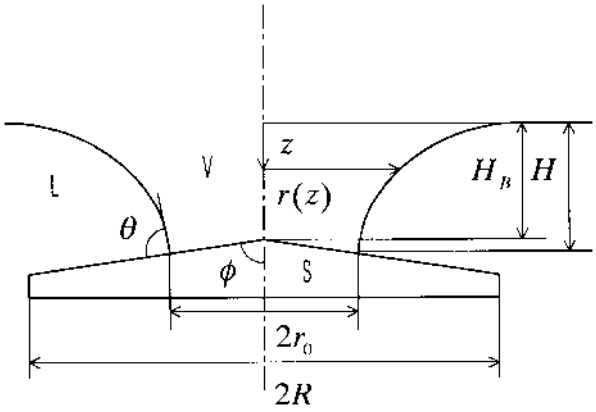

FIG. 18 Schematic of axisymmetric meniscus attached to an upward cone surface.

reference state, the nondimensional energy $\overline{E}_W$ required for the the three-phase contact line to wet the surface to radius $\bar{r}_0$ in the inward direction can be calculated as

$$\overline{E}_W = \frac{\pi(\bar{r}_0^2 - \overline{R}^2)}{\sin\phi}\cos\theta_A,$$

As stated previously in the derivation of Eq. (42b), the constant term is omitted from the above equation for the purpose of simplicity:

$$\overline{E}_W = \frac{\pi\bar{r}_0^2}{\sin\phi}\cos\theta_A. \tag{45}$$

The total energy of the system shown in Fig. 18 is obtained from the sum of Eqs. (40), (41), and (45). Fig. 19 shows the calculated results for the advancing contact angle $\theta_A = 90^\circ$ as an example. The system exhibits both maximum and minimum energies at $\theta = 90^\circ$ for $\overline{H}_B$ smaller than a critical depth, similarly as shown in Fig. 17. When $\overline{H}_B$ is larger than 0.590, the energy has no extreme value and increases monotonically with $\bar{r}_0$, as shown by Fig. 19b. Hence the liquid spreads and wets the entire surface of the upward cone. We can obtain the critical depth $\overline{H}_B$ for each advancing contact angle. It is possible to measure θ_A by the same method as for the receding contact angle if we reverse the cone surface.

D. Measuring Method of Contact Angles and Surface Tension Using the Cone Surface

As stated above, we theoretically discussed the unstable wetting behavior of an axisymmetric meniscus attached to a cone surface. It was suggested that

Copyright n 2004 by Marcel Dekker, Inc. All Rights Reserved.

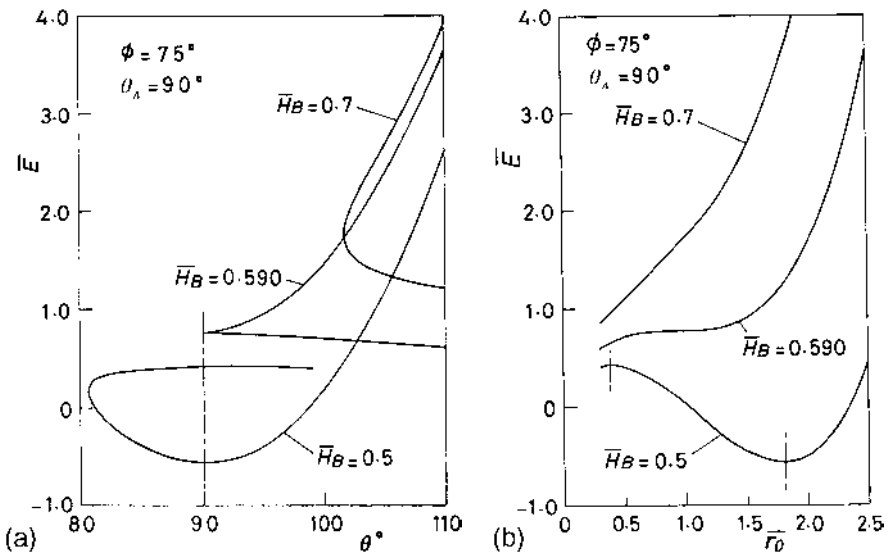

FIG. 19 Energy curve for various cone depths $\overline{H}_B$ shown in Fig. 18. The system has no energy minimum and becomes unstable when $\overline{H}_B$ is larger than 0.590.

contact angles could be obtained by simple measurement of the critical height at which the instability occurs [65]. In this section, the contact angles are actually measured according to the principle suggested here. Fig. 20 shows the functional relation between the critical height of the cone vertex $\overline{H}_{Bcr}$ and contact angles θ_R and θ_A for a cone of $\phi = 85°$. The theoretical curve shown in Fig. 20 was obtained from the height at which the energy has no extreme values, as shown in Fig. 17 or Fig. 19. The contact angles can be calculated from Fig. 20 if the critical height or depth $\overline{H}_{Bcr}$ is measured.

In order to confirm the principle stated above, a rather simple experiment was carried out. The experimental apparatus used here is schematically depicted in Fig. 21. The solid cone surface (1) is drawn from the liquid bath (3) and the critical height at which the meniscus falls off is measured using a micrometer (4). The bottom surface of (3) was chosen as the reference position for the measurement of height. In this experiment, we used a capacitance probe (6) to measure the position of the liquid surface [66]. In order to confirm the method proposed here, the meniscus shape was photographed by a camera (5) from the side of (3) and contact angles were read from the photograph for each measurement of critical height. Water and ethanol solution were used as test liquids. Table 2 shows the properties of the test liquids and the range of temperature in the experiment. The temperature was checked at each measurement of contact angles. The test cone surface was

Copyright n 2004 by Marcel Dekker, Inc. All Rights Reserved.

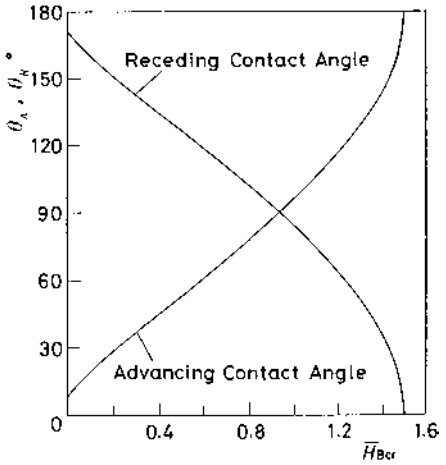

FIG. 20 The relation between contact angles and the critical cone height $\overline{H}_{Bcr}$ (ϕ = 85°) at which the system becomes unstable as shown in Figs. 18 and 19.

prepared using a lathe. In this experiment, solid surfaces of different materials were prepared: brass, duralumin, vinyl chloride, and Teflon. Each test solid, except Teflon, was finished by both turning and polishing to vary the surface roughness.

First, the critical height was roughly measured. Then, the cone surface was raised more slowly near the critical position determined above and $\overline{H}_{Bcr}$, at which the instability occurred, was precisely measured. The measurements of $\overline{H}_{Bcr}$'s were repeated five or six times under each set of experimental

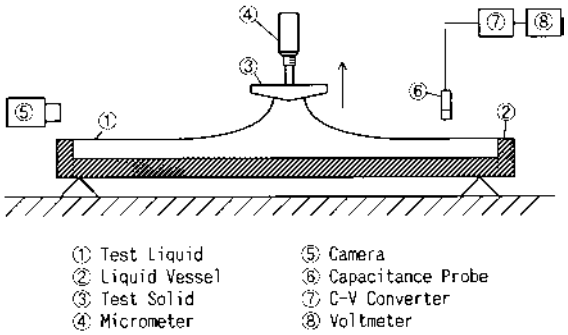

FIG. 21 Schematic of experimental apparatus to measure contact angles using a cone surface.

Copyright n 2004 by Marcel Dekker, Inc. All Rights Reserved.

TABLE 2 Properties of Test Liquids

Liquid	Temperature (°C)	Density (kg/m^3)	Surface tension (N/m)
Water	12–19	998–1000	0.0736–0.0743
Ethanol solution	12–19	965–975	0.0368–0.0428

conditions. The scatter of critical height values was about 5/1000 mm, which confirmed the good reproducibility of the measurement.

Fig. 22 shows the results of measurements. The theoretical curve depicted in the figure is the same as that in Fig. 20. Each experimental point is a plot of the measured critical height $\overline{H}_{\mathrm{Bcr}}$ and the corresponding contact angle obtained from the photograph. Hence the experimental points would lie on the theoretical curve if the contact angles obtained by the method proposed here coincided with those from the photograph. Fig. 22 shows rough agreement between experimental points and the theoretical curve, which indicates the feasibility of measurement using the method proposed here. The disagreement with the curve may be mainly due to the difficulty of measurement of contact angles from the photograph since the meniscus attaches to a curved cone surface. The agreement indicated by Fig. 22 also shows the validity of the discussion given in the preceding section, where we analyzed the unstable wetting behavior based on Eq. (9) assumed in Section I.

Although only contact angles were measured here, the liquid–vapor interfacial tension could also be measured based on the same principle. A glass cone with zero contact angle with liquids could be used, instead of the test solids described above, in the measurement of interfacial tension. The critical height corresponding to $\theta_{\mathrm{R}} = 0°$ can be obtained as $\overline{H}_{\mathrm{Bcr}} = 1.508$, from Fig. 20, for $\phi = 85°$. This relation can be rewritten in the dimensional form, using the capillary constant defined by Eq. (13), as

$$H_{\mathrm{Bcr}} = 1.508\sqrt{\frac{\sigma_{\mathrm{LV}}}{\Delta\rho g}}. \tag{46}$$

If we measure the critical height H_{Bcr} when the liquid falls off the glass cone surface, the liquid–vapor interfacial tension can be calculated from Eq. (46).

III. METHOD OF APPLYING GEOMETRICAL INSTABILITY OF THE TWO-DIMENSIONAL MENISCUS

In the preceding section, we discussed the method of applying the thermodynamic instability of an axisymmetric meniscus attached to a cone surface. The

Copyright n 2004 by Marcel Dekker, Inc. All Rights Reserved.

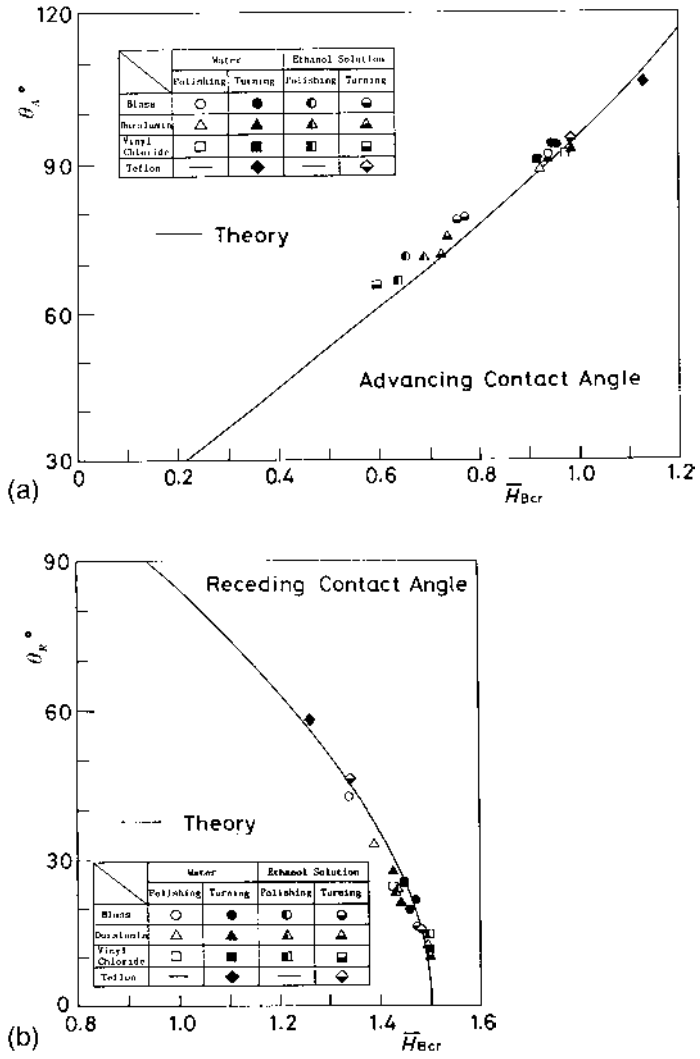

FIG. 22 Comparison of contact angles measured by the proposed method with those from a photograph: (a) advancing contact angle; (b) receding contact angle.

Copyright n 2004 by Marcel Dekker, Inc. All Rights Reserved.

method has the merit of enabling the contact angle or liquid–vapor interfacial tension to be obtained by direct measurement of the critical height. When the method is applied to the measurement of contact angles, however, it may not be convenient to prepare a cone surface as a test piece every time. Practically, it is desirable to use a plate or circular cylinder for the measurement. In this section, we discuss another measuring method of contact angles and interfacial tension, in which the instability of a two-dimensional meniscus is applied in a manner different from that proposed in the preceding section [67].

A. Principle of the Method

Fig. 23 schematically shows the principle of the method of using a circular cylinder as the test solid. S, L, and V in the figure indicate solid, liquid, and vapor phases, respectively. The cylinder held horizontally is first immersed and then slowly drawn from the liquid bath. We can see a pair of two-dimensional menisci formed under the cylinder, as shown in Fig. 23a. As the cylinder is raised to a certain critical height, the waists of the two meniscus curves contact each other and the liquid breaks off from the solid surface. The geometry of the two-dimensional meniscus can be determined from the Laplace equation (11) and the contact angle as a boundary condition, as mentioned in Section I. Hence we could calculate the contact angle using the

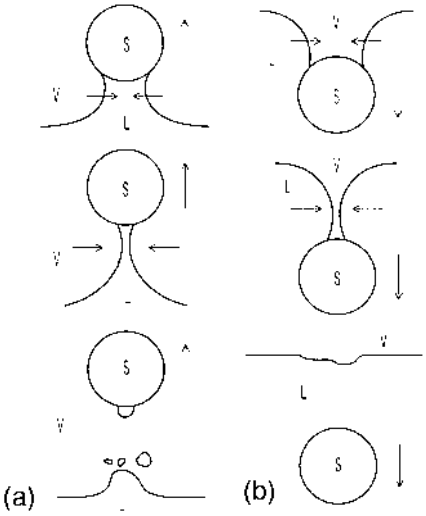

FIG. 23 Principle of the method for the measurement of contact angle using circular cylinder based on geometrical instability of two-dimensional meniscus: (a) receding contact angle; (b) advancing contact angle.

Copyright n 2004 by Marcel Dekker, Inc. All Rights Reserved.

critical height at which the break-off of the meniscus occurs, as shown in Fig. 23a. Since the three-phase contact line recedes on the solid surface as the cylinder is raised in the case of Fig. 23a, the receding contact angle θ_R would be obtained by measuring the critical height. On the other hand, when the cylinder is inversely immersed into a liquid bath, as shown in Fig. 23b, the meniscus curves contact each other at a certain critical depth. In this case, the meniscus is broken and the liquid wets the entire surface of the cylinder. Since the contact line advances on the solid surface as the cylinder is immersed, we can obtain the advancing contact angle from the measurement of the critical depth.

Fig. 24 shows the principle of the method in a similar manner, for a plate used as the test solid. As shown in Fig. 24a, the test plate S_1 is fixed onto the inclined surface of support S_2 and is drawn up from the liquid bath. The two-dimensional meniscus formed under S_1 gradually approaches the support wall as the test plate is raised. The waist of the meniscus curve contacts the wall at a critical height and the meniscus breaks off from the solid surface. In a similar manner to that for the horizontal cylinder, we could calculate the receding contact angle from the measured critical height. Fig. 24b shows the measurement of the advancing contact angle. In this case, the plate and support are reversed, as shown in the figure. The three-phase contact line advances

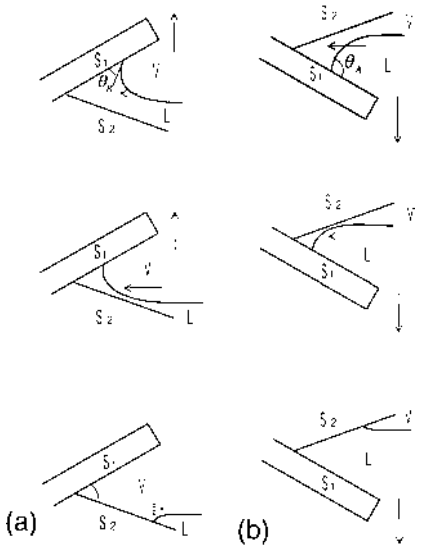

FIG. 24 Principle of the method for the measurement of contact angle using tilted plate based on geometrical instability of two-dimensional meniscus: (a) receding contact angle; (b) advancing contact angle.

Copyright n 2004 by Marcel Dekker, Inc. All Rights Reserved.

gradually on the test plate as S_1 and S_2 are slowly immersed into the liquid. At a critical depth of the plate, the liquid contacts the support wall and wets the entire surface, as shown in the figure. The advancing contact angle could be calculated by measuring the critical depth.

B. Relation Between Critical Height and Contact Angle

As mentioned above, it is, in principle, possible to obtain contact angles by measuring the critical height or depth at which the geometrical instability of a two-dimensional meniscus occurs. Here the relationship between the critical height of cylinder or plate and the contact angles is discussed theoretically. First, let us consider the circular cylinder shown in Fig. 25. In the figure, the x- and z-axes are taken to be the direction of the stationary liquid surface and the vertical direction through the cylinder center, respectively. The height of the cylinder bottom H_B from the stationary liquid surface shown in Fig. 25 is used as the measuring height of the cylinder. In this section, we use the nondimensional solution of the Laplace equation, i.e., Eqs. (14) and (15), which determines the geometry of the two-dimensional meniscus. The unknown integral constant C in Eq. (14) should be determined from the boundary condition. Since the meniscus is in contact with the cylinder of radius R at the receding contact angle θ_R, as shown in Fig. 25, Eq. (14) should satisfy the boundary condition

$$x = x_0 = R\sin\,\phi \text{ at } \psi = (\phi + \theta_R),$$

where x_0 and ϕ indicate the coordinate at the attachment point of the meniscus and the angle between the z-axis and the cylinder radius at the attachment point, respectively, as seen in Fig. 25. ψ is the inclination of the

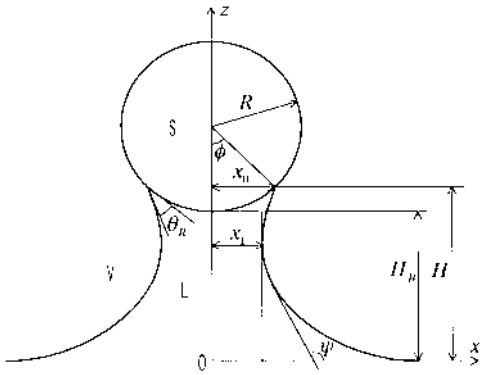

FIG. 25 Schematic of two-dimensional meniscus attached to a circular cylinder.

Copyright n 2004 by Marcel Dekker, Inc. All Rights Reserved.

meniscus curve from the x-axis. Using the capillary constant defined by Eq. (13), the above boundary condition is rewritten in the nondimensional form as

$$\bar{x} = \bar{x}_0 = \overline{R} \sin \phi \text{ at } \psi = \phi + \theta_R.$$

Equation (14) can be rewritten as below if the constant C is calculated from the boundary condition.

$$\begin{aligned} \bar{x} = & \ln\left\{\frac{1+\sin\left(\frac{\psi}{2}\right)}{\cos\left(\frac{\psi}{2}\right)}\right\} - \ln\left\{\frac{1+\sin\left(\frac{\theta_R+\phi}{2}\right)}{\cos\left(\frac{\theta_R+\phi}{2}\right)}\right\} \\ & + 2\left\{\sin\left(\frac{\theta_R+\phi}{2}\right) - \sin\left(\frac{\psi}{2}\right)\right\} + \overline{R}\sin\phi \end{aligned} \tag{47}$$

The angle ϕ in the above equation gradually decreases with increasing cylinder height. Finally, when the waists of two meniscus curves contact each other, the x coordinate at $\psi = \pi/2$, i.e., x_1 shown in Fig. 25, becomes zero. Substituting $\psi = \pi/2$ into Eq. (47) and taking $\bar{x} = \bar{x}_1 = 0$, the following relation holds for the angle ϕ when the meniscus breaks off from the solid surface:

$$\begin{aligned} & \overline{R}\sin\phi - \ln\left\{\frac{1+\sin\left(\frac{\theta_R+\phi}{2}\right)}{\cos\left(\frac{\theta_R+\phi}{2}\right)}\right\} + 2\sin\left(\frac{\theta_R+\phi}{2}\right) \\ & + \ln\left(1+\sqrt{2}\right) - \sqrt{2} = 0 \end{aligned} \tag{48}$$

On the other hand, the meniscus height at the position of attachment to the cylinder can be calculated from Eq. (15) as

$$\overline{H} = 2\cos\left(\frac{\theta_R+\phi}{2}\right). \tag{49}$$

Using the solution of Eq. (48) as ϕ_R in Eq. (49), the height of the cylinder bottom $\overline{H}_{Bcr}$ under the critical condition can be obtained as follows from a simple geometrical consideration:

$$\overline{H}_{Bcr} = 2\cos\left(\frac{\theta_R+\phi_R}{2}\right) - \overline{R}(1-\cos\phi_R) \quad (\theta_R \le 90^\circ) \tag{50}$$

The above equation gives the critical height for receding contact angles θ_R less than 90°. If θ_R becomes greater than 90°, the liquid falls off when the vertexes of the two meniscus curves contact each other exactly at the bottom of the

Copyright n 2004 by Marcel Dekker, Inc. All Rights Reserved.

cylinder, as shown in Fig. 26. Since the inclination of the meniscus at the vertex is equal to the receding contact angle θ_R, the critical height of the cylinder can be calculated simply by using θ_R instead of ψ in Eq. (15) as

$$\overline{H}_{Bcr} = 2\cos\left(\frac{\theta_R}{2}\right) \quad (\theta_R > 90^\circ). \tag{51}$$

The relationship for the advancing contact angle can be obtained in a similar manner as described above. The details are not discussed here to avoid repetition. We can readily obtain the relationship between the critical depth and the advancing contact angle θ_A if we use $(\pi-\theta_A)$ instead of θ_R in Eqs. (48), (50), and (51). Equation (48) is rewritten for θ_A as

$$\overline{R}\sin\phi_A - \ln\left\{\frac{1+\cos\left(\frac{\theta_A-\phi_A}{2}\right)}{\sin\left(\frac{\theta_A-\phi_A}{2}\right)}\right\} + 2\cos\left(\frac{\theta_A-\phi_A}{2}\right) + \ln\left(1+\sqrt{2}\right) - \sqrt{2} = 0. \tag{52}$$

Using the solution of the above equation as ϕ_A, the following relations between the critical depth and the advancing contact angle can be given as

$$\overline{H}_{Bcr} = 2\sin\left(\frac{\theta_A-\phi_A}{2}\right) - \overline{R}(1-\cos\phi_A) \quad (\theta_A \geq 90^\circ) \tag{53}$$

$$\overline{H}_{Bcr} = 2\sin\frac{\theta_A}{2} \quad (\theta_A < 90^\circ) \tag{54}$$

Next, let us consider the relationship for a plate used as the test solid. As shown in Fig. 27, we take the height of intersection B of test plate S_1 with support S_2 as the measuring height H_B. The z-axis is taken to be the vertical

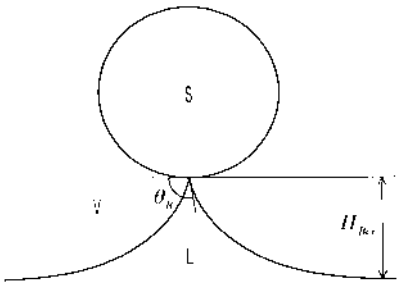

FIG. 26 Critical condition for receding contact angle θ_R larger than 90° at which the meniscus falls off the cylinder surface.

Copyright n 2004 by Marcel Dekker, Inc. All Rights Reserved.

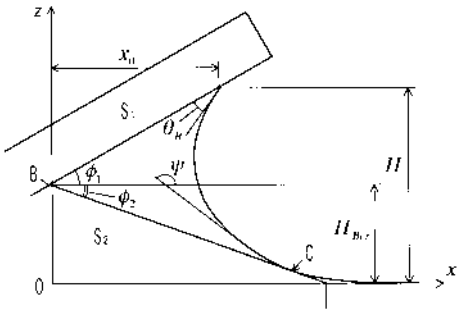

FIG. 27 Schematic of critical condition at which meniscus contacts the surface of the support S_2.

direction through B. Fig. 27 indicates the critical condition just as the meniscus curve contacts the S_2 wall at C. The critical height of B, i.e., $\overline{H}_{\mathrm{Bcr}}$, can be written as follows based on a simple geometrical consideration:

$$\begin{aligned}\overline{H}_{\mathrm{Bcr}} &= \overline{H} - \bar{x}_0 \tan \phi_1 \\ &= 2 \cos\left(\frac{\theta_{\mathrm{R}} + \phi_1}{2}\right) - \bar{x}_0 \tan \phi_1\end{aligned} \tag{55}$$

Equation (15) was used to obtain the meniscus height $\overline{H}$. As seen in Fig. 27, $\bar{x}_0$ and ϕ_1 indicate the nondimensional coordinate of the meniscus at the attachment position and the inclination of the test plate, respectively. The gradient of the meniscus curve becomes equal to that of the solid wall (i.e., ϕ_2 shown in the figure) at C. Hence the coordinate of the contact, $\bar{z}_{\mathrm{C}}$, can be calculated by using $(\pi - \phi_2)$ instead of ψ in Eq. (15) as

$$\bar{z}_{\mathrm{C}} = 2 \sin\left(\frac{\phi_2}{2}\right). \tag{56}$$

Using the above equation, the $\bar{x}$ coordinate of the contact, $\bar{x}_{\mathrm{C}}$, can be obtained geometrically as

$$\bar{x}_{\mathrm{C}} = \left\{ \overline{H}_{\mathrm{Bcr}} - 2 \sin\left(\frac{\phi_2}{2}\right) \right\} \frac{1}{\tan \phi_2}. \tag{57}$$

Now we use Eq. (14) for the meniscus profile. When $\psi = \pi - \phi_2$ is substituted into the right-hand side of Eq. (14), the result should be equal to Eq. (57). Hence we can determine the integral constant C in Eq. (14) under the critical condition. Substituting the calculated C and $\psi = \theta_{\mathrm{R}} + \phi_1$ at the attachment

Copyright n 2004 by Marcel Dekker, Inc. All Rights Reserved.

position of the meniscus to the test plate S_1 into Eq. (14) again, $\bar{x}_0$ shown in Fig. 27 can be obtained as follows:

$$\bar{x}_0 = \ln\left\{\frac{1+\sin\left(\frac{\theta_R+\phi_1}{2}\right)}{\cos\left(\frac{\theta_R+\phi_1}{2}\right)}\right\} - \ln\left\{\frac{1+\cos\frac{\phi_2}{2}}{\sin\frac{\phi_2}{2}}\right\} - 2\sin\left(\frac{\theta_R+\phi_1}{2}\right) + \frac{\overline{H}_{Bcr}}{\tan\phi_2} + \frac{1}{\cos\frac{\phi_2}{2}} \tag{58}$$

Finally, the critical height $\overline{H}_{Bcr}$ shown in Fig. 27 is written as follows if Eq. (58) is inserted into Eq. (55):

$$\overline{H}_{Bcr} = 2\cos\left(\frac{\theta_R+\phi_1}{2}\right) - \frac{2\tan\phi_1}{\tan\phi_1+\tan\phi_2}\left[\cos\left(\frac{\theta_R+\phi_1}{2}\right) - \sin\frac{\phi_2}{2} - \left\{\sin\left(\frac{\theta_R+\phi_1}{2}\right) - \cos\frac{\phi_2}{2} - \frac{1}{2}\ln\left(\frac{1+\sin\left(\frac{\theta_R+\phi_1}{2}\right)}{\cos\left(\frac{\theta_R+\phi_1}{2}\right)}\right) + \frac{1}{2}\ln\left(\frac{1+\cos\frac{\phi_2}{2}}{\sin\frac{\phi_2}{2}}\right)\right\}\tan\phi_2\right] \tag{59}$$

When $(\theta_R+\phi_1)$, i.e., the inclination of the meniscus from the horizontal at the test plate, becomes greater than $(\pi-\phi_2)$, the meniscus does not contact support S_2 until it reaches B, as shown in Fig. 28. In this case, the three-phase contact line might be trapped at the corner between S_1 and S_2 because the tip of S_2 would be slightly rounded. The meniscus would not break off

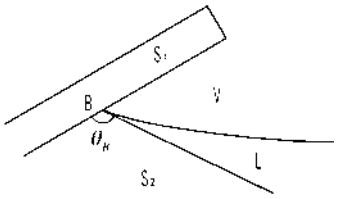

FIG. 28 Critical condition for receding contact angle θ_R larger than $[\pi-(\phi_1+\phi_2)]$: the three phase line is trapped at the corner between S_1 and S_2.

Copyright n 2004 by Marcel Dekker, Inc. All Rights Reserved.

from the plate even if the plate was raised higher than the critical condition. Hence the measurement applying Eq. (59) should be limited to the following range of receding contact angles:

$$\theta_R < \pi - (\phi_1 + \phi_2) \tag{60}$$

For the measurement of advancing contact angle θ_A, the test plate is immersed inversely into a liquid bath, as shown in Fig. 24b. The critical depth of the test plate can be obtained in the same manner as for the receding contact angle, so we do not discuss the details here. The relationship between the critical depth at which instability occurs and θ_A can be calculated if we use $(\pi - \theta_A)$ instead of θ_R in Eq. (59) as

$$\begin{aligned}\overline{H}_{Bcr} = 2\ \sin\left(\frac{\theta_A - \phi_1}{2}\right) - \frac{2\ \tan\phi_1}{\tan\phi_1 + \tan\phi_2}\Bigg[\sin\left(\frac{\theta_A - \phi_1}{2}\right) \\ -\sin\frac{\phi_2}{2} - \Bigg\{\cos\left(\frac{\theta_A - \phi_1}{2}\right) - \cos\frac{\phi_2}{2} - \frac{1}{2}\ln\left(\frac{1 + \cos\left(\frac{\theta_A - \phi_1}{2}\right)}{\sin\left(\frac{\theta_A - \phi_1}{2}\right)}\right) \\ + \frac{1}{2}\ln\left(\frac{1 + \cos\frac{\phi_2}{2}}{\sin\frac{\phi_2}{2}}\right)\Bigg\}\tan\phi_2\Bigg]\end{aligned} \tag{61}$$

According to the same reason as for Eq. (60), the measurement of the advancing contact angle is limited to the following region:

$$\theta_A > \phi_1 + \phi_2 \tag{62}$$

Fig. 29 shows the relationship between θ_R or θ_A and $\overline{H}_{Bcr}$ calculated by Eqs. (50), (51), (53), and (54) for cylinder and by Eqs. (54) and (61) for plate. The calculated results are presented in the figures for several values of cylinder radius $\overline{H}$ and inclinations ϕ_1 and ϕ_2. As seen in the figures, each critical height or depth corresponds to one contact angle, which indicates the validity of the method. In Fig. 29a for a circular cylinder, each curve for various $\overline{R}$'s converges to one curve in the region of $\theta_R > 90^\circ$ or $\theta_A < 90^\circ$. This is because the meniscus falls off the solid surface exactly at the bottom of the cylinder, as described by Fig. 26, and the critical height is not dependent on the cylinder radius. In Fig. 29a, we can see that the gradient of the theoretical curves becomes steep close to $\theta_R = 0^\circ$ and $\theta_A = 180^\circ$ for all cylinder radii. This is due to the fact that the gradient of the meniscus curve becomes nearly horizontal

Copyright n 2004 by Marcel Dekker, Inc. All Rights Reserved.

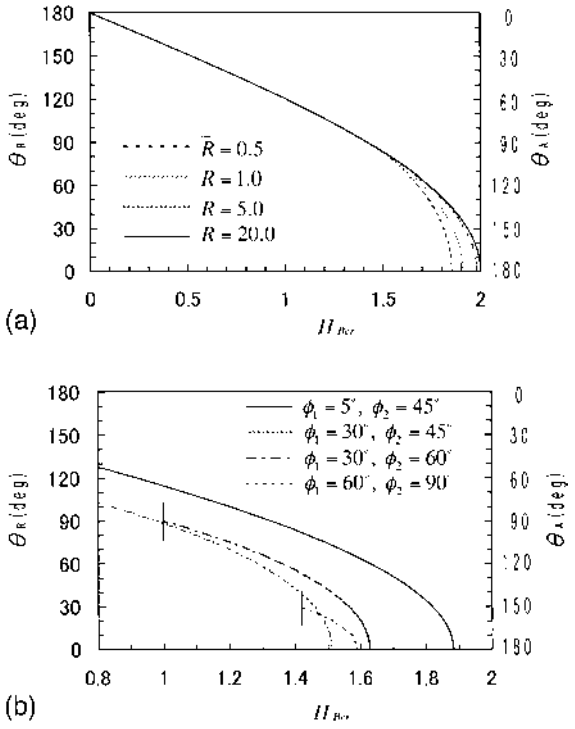

FIG. 29 Theoretical relation between contact angle and nondimensional critical height of (a) cylinder and (b) tilted plate.

at the attachment point for those contact angles. Hence the critical height varies only slightly with the change of contact angle, i.e., $dH/d\theta_R \approx 0$. This might be evident if we calculate $(dH/d\theta)$ at $\theta = 0°$ from Eq. (22), which determines the height of the meniscus attached to a horizontal plate. The above fact indicates an inaccuracy in the measurement around such contact angles. A similar tendency is observed in Fig. 29b for the plate used as the test solid. However, the accuracy can be improved if we use the test plate and support with large inclination in order to make the gradient of the meniscus curve steep at the attachment point. In fact, the theoretical curves of $\phi_1 = 60°$ and $\phi_2 = 90°$ have a gentle gradient near $\theta_R = 0°$ and $\theta_A = 180°$ compared with other curves, as shown in Fig. 29b. However, the region in which measurement is possible becomes more limited as ϕ_1 or ϕ_2 increases, as described by Eq. (60) or Eq. (62). The vertical bar | in Fig. 29b shows the limit of measurement. It would be desirable to prepare some supports with different inclinations to measure various contact angles with sufficient accuracy.

Copyright n 2004 by Marcel Dekker, Inc. All Rights Reserved.

C. Critical Height for Measurement of the Liquid–Vapor Interfacial Tension

In a similar manner to the measurement using the cone surface described in Section II, it is possible to measure the liquid–vapor interfacial tension based on the same principle as for the contact angle, if a glass cylinder or plate is used as the test solid.

In the measurement using the glass cylinder, substitution of $\theta_R = 0°$ into Eq. (48) leads to the following relation in dimensional form, through the use of Eq. (13).

$$\sqrt{\frac{\Delta\rho g}{\sigma_{LV}}}R \sin\phi - \ln\left(\frac{1+\sin\frac{\phi}{2}}{\cos\frac{\phi}{2}}\right) + 2\sin\frac{\phi}{2} + \ln(1+\sqrt{2}) - \sqrt{2} = 0 \quad (63)$$

The above equation gives the angle ϕ shown in Fig. 25 at which the meniscus breaks off from the cylinder surface. We can obtain the solution of Eq. (63) numerically for an arbitrary value of liquid–vapor interfacial tension if the density of the test liquid is known. Assuming the solution of Eq. (63) to be ϕ_T, Eq. (50) can be rewritten in dimensional form after the insertion of $\theta_R = 0°$ as

$$H_{Bcr} = 2\sqrt{\frac{\sigma_{LV}}{\Delta\rho g}}\cos\frac{\phi_T}{2} - R(1 - \cos\phi_T). \quad (64)$$

The critical height corresponding to the liquid–vapor interfacial tension can be calculated by the above equation.

For the plate, we similarly substitute $\theta_R = 0°$ into Eq. (59) and rewrite the equation in dimensional form. The relation between the liquid–vapor interfacial tension and the critical height H_{Bcr} can be written as

$$\begin{aligned}\sqrt{\frac{\sigma_{LV}}{\Delta\rho g}} = \frac{1}{2}H_{Bcr}\Bigg[\cos\frac{\phi_1}{2} - \frac{\tan\phi_1}{\tan\phi_1+\tan\phi_2}\Bigg\{\cos\frac{\phi_1}{2} - \sin\frac{\phi_2}{2} \\ - \Bigg(\sin\frac{\phi_1}{2} - \cos\frac{\phi_2}{2} - \frac{1}{2}\ln\left(\frac{1+\sin\frac{\phi_1}{2}}{\cos\frac{\phi_1}{2}}\right) \\ + \frac{1}{2}\ln\left(\frac{1+\cos\frac{\phi_2}{2}}{\sin\frac{\phi_2}{2}}\right)\Bigg)\tan\phi_2\Bigg\}\Bigg]^{-1}\end{aligned} \quad (65)$$

Fig. 30 shows the relation between $(\sigma_{LV}/\Delta\rho)$ and H_{Bcr} for the cylinder and the plate. As seen in the figure, the liquid–vapor interfacial tension can be

Copyright n 2004 by Marcel Dekker, Inc. All Rights Reserved.

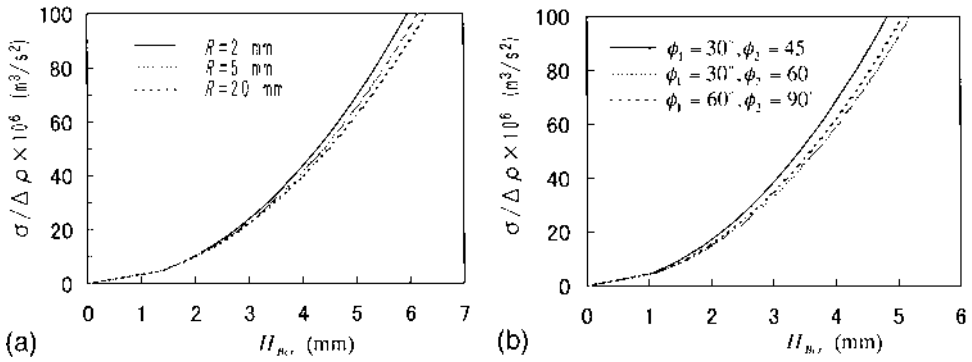

FIG. 30 Theoretical relation between liquid–vapor interfacial tension and critical height: (a) circular cylinder; (b) tilted plate.

obtained by measuring the critical height, in a same manner as for the contact angle. Although there were some regions in which the measurement of the contact angle was inaccurate, as mentioned in the preceding section, it is possible to measure the liquid–gas interfacial tension correctly over its entire range for both cylinders and plates, as shown in Fig. 30.

D. Experiment

The results described in Sections III.B and III.C indicate that it is possible to measure the liquid–vapor interfacial tension as well as the contact angle using the same apparatus if the test cylinder or plate is changed according to the desired measurement. An experiment was carried out to actually measure contact angles and interfacial tensions based on the principle described in the preceding sections. Since the main purpose here is to confirm the validity of the principle and to perform measurement using a simple apparatus, the accuracy is not of high concern in this experiment.

Fig. 31 shows the schematic of the experimental apparatus used. The apparatus is similar to, but slightly modified from, that used for the work described in Section II.D. The test cylinder or plate (4) is attached to the feeding device and drawn from vessel (1) filled with test liquid (2). The critical height H_{Bcr} at which the liquid falls off from the test surface is measured by a micrometer (3) from the bottom surface of (1) as the reference plane. For the measurement of the advancing contact angle, the cylinder or plate is inversely immersed into the test liquid and the critical depth is measured in the same manner. The distance between the liquid surface and the reference plane is measured by the needle contact method [68], which is simple compared with

Copyright n 2004 by Marcel Dekker, Inc. All Rights Reserved.

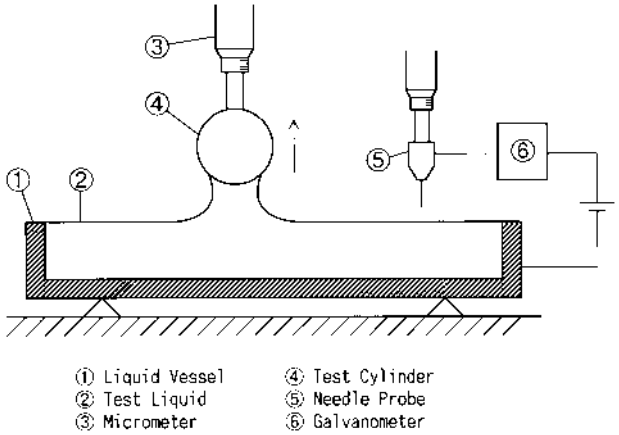

FIG. 31 Schematic of experimental apparatus for the measurement of contact angle and liquid–vapor interfacial tension.

the capacitance probe method used in Section II.D. A probe with a thin needle is fed by a micrometer. When the tip of the needle contacts the liquid surface or the bottom of the vessel (1), a simple circuit is closed, as shown in Fig. 31. The position of the liquid surface can be measured by the micrometer when a signal from a galvanometer is detected. Although a liquid without conductivity is used, we can determine the position to within 1/100 mm by the naked eye, using a mirror to observe when the needle comes into contact with the liquid surface [35]. The liquid meniscus formed under a solid surface may not remain two-dimensional. Hence, in this experiment, thin plates are fixed to both ends of the test cylinder or plate, as shown in Fig. 32, to maintain the two-dimensionality of the meniscus. The liquid near the ends is fixed by the plates and does not shrink to the middle part of the cylinder. Although the liquid layer may become thick and the meniscus loses two-dimensionality

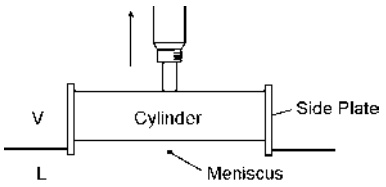

FIG. 32 Side view of the measurement of critical height using circular cylinder: side plates are fixed on the ends of the cylinder to maintain the two-dimensionality of the meniscus.

Copyright n 2004 by Marcel Dekker, Inc. All Rights Reserved.

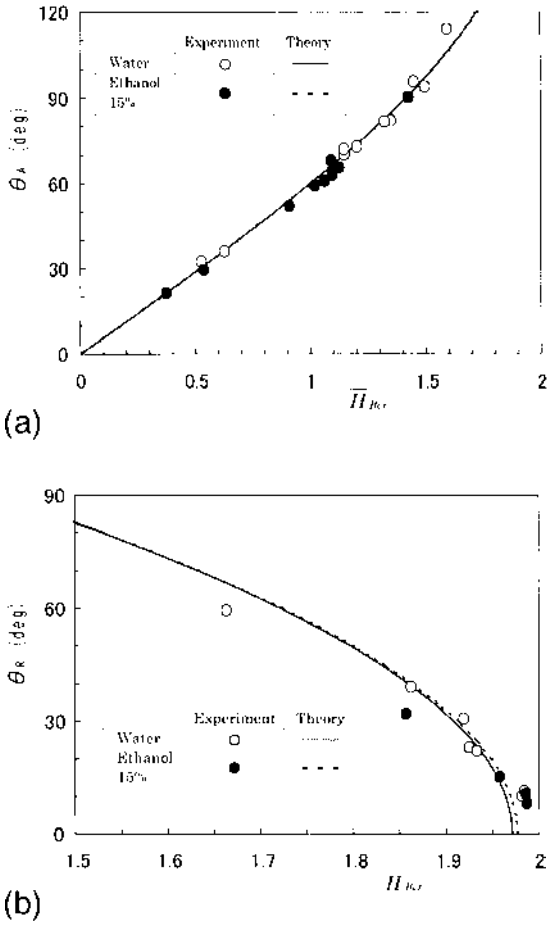

FIG. 33 Comparison of contact angles measured by the proposed method using circular cylinder with those from a photograph: (a) advancing contact angle; (b) receding contact angle.

near the end plates, the critical height can be measured correctly because the instability of the meniscus, as described in Figs. 23 and 24, occurs around the central region of the cylinder where the meniscus is two-dimensional. The length of the test cylinder or plate should be about 10 times the meniscus height in order to maintain two-dimensionality in the central region.

Six kinds of solid surfaces were prepared for the measurement of the contact angle: brass, duralumin, stainless steel, vinyl chloride, nylon, and Teflon. In a similar manner as the method using the cone surface described in

Copyright n 2004 by Marcel Dekker, Inc. All Rights Reserved.

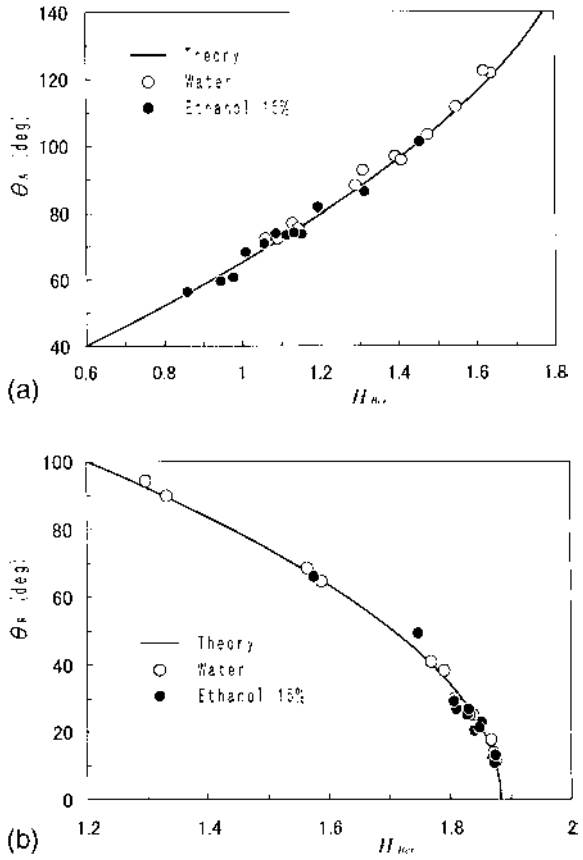

FIG. 34 Comparison of contact angles measured by the proposed method using tilted plate with those by a commercially available contact angle meter: (a) advancing contact angle; (b) receding contact angle.

Section II.D, each material was finished by several methods, such as lathing and polishing, in order to measure contact angles for various surface roughnesses. The test liquids were water and 15% ethanol solution for the measurement of the contact angle and water, four kinds of ethanol solution of different concentrations, and two kinds of machine oils for the measurement of the liquid–vapor interfacial tension.

For comparison, the contact angle was also measured from a photograph for the cylinder and by using a commercially available contact angle meter (Kyowa Kaimen Kagaku CA-A type) for the plate, in which the contact angle of a drop is measured using a telescope with a goniometer. The liquid–vapor interfacial tension was also measured by the Wilhelmy method using a

Copyright n 2004 by Marcel Dekker, Inc. All Rights Reserved.

commercially available surface tension meter (Kyowa Kaimen Kagaku CBVP-A3 type).

The measured results of contact angles for the cylinder and for the plate are shown in Figs. 33 and 34, respectively. The experimental points in the figures are plotted in the same manner as in Fig. 22 in Section II.D, i.e., by using the measured critical height $\overline{H}_{\mathrm{Bcr}}$ (abscissa) and the contact angle measured from a photograph or using a contact angle meter (ordinate). If the results measured by the two different methods agreed with each other, the experimental points should lie on the theoretical curves obtained in the preceding section, as shown in the figures. There is some scatter of data in Fig. 33b for the receding contact angle measured using a cylinder. This may be due to error in the photograph method because it is difficult to measure contact angles on a

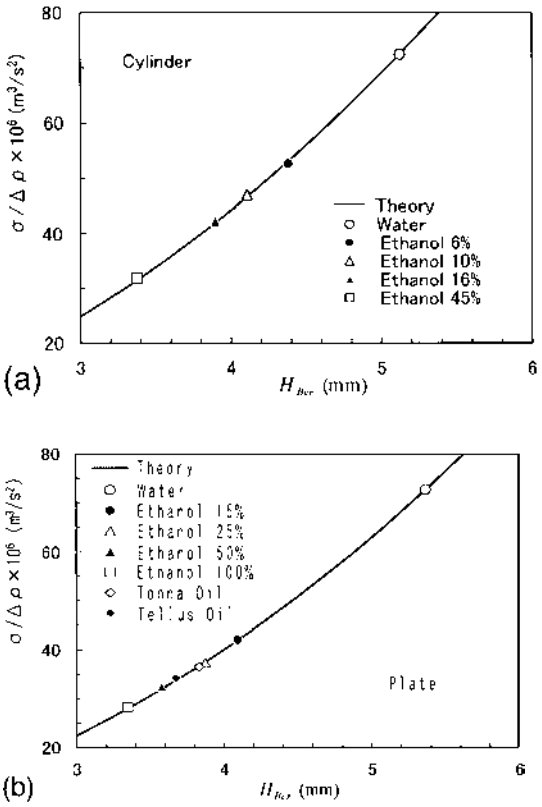

FIG. 35 Comparison of liquid–vapor interfacial tension measured by the proposed method with those by a commercially available surface tensiometer: (a) circular cylinder; (b) tilted plate.

Copyright n 2004 by Marcel Dekker, Inc. All Rights Reserved.

curved surface. For the plate used as the test solid, on the other hand, the theoretical curves fit the data well for both receding and advancing contact angles, as shown in Fig. 34. The discrepancy from the curve is about 2°, which is roughly the same value as the error in the direct method using a goniometer. The error in critical height measured using the apparatus shown in Fig. 31 is about 1/100 mm, which corresponds to less than 10^{-2} in nondimensional height $\overline{H}_{\mathrm{Bcr}}$ and to the error of $\pm 1°$ in the contact angle at $\theta_{\mathrm{R}} = 45°$.

Fig. 35 shows the experimental results of the interfacial tension σ_{LV} measured by the same method as the contact angle, using a glass cylinder or plate as test solid. The experimental points in the figures are plotted using σ_{LV} measured by the Wilhelmy method and critical heights. As shown in the figures, it is possible to measure the interfacial tension by the method proposed here. The discrepancy between experimental points and the theoretical curve is less than 0.2×10^{-3} (N/m), which roughly corresponds to the degree of error in the Wilhelmy method used in this experiment. The error of 1/100 mm in the critical height mentioned above corresponds to 0.2×10^{-3} (N/m) in liquid–vapor interfacial tension. It is possible to measure the interfacial tension by the method proposed here to about the same accuracy as the Wilhelmy method.

IV. DISCUSSION

Two kinds of methods were proposed for the measurement of the contact angle and the liquid–vapor interfacial tension; one applies the thermodynamic instability and the other is based on the geometrical instability of the meniscus attached to a solid surface. In Section II, the thermodynamic instability of an axisymmetric meniscus formed under a cone was analyzed based on the assumption discussed in Section I, which makes it possible to calculate the energy change due to the macroscopic wetting behavior of the three-phase contact line on a rough and heterogeneous surface. The relation between the contact angle or liquid–vapor interfacial tension and the critical height of a cone when the axisymmetric meniscus spontaneously falls off the solid surface due to thermodynamic instability was obtained theoretically. The method proposed in Section III is based on the phenomenon that the two-dimensional meniscus breaks off from a circular cylinder or plate at a critical height. The contact angle and the liquid–vapor interfacial tension can be obtained simply by measuring the critical height in both methods without the need for any optical or dynamical apparatus.

In the method applying thermodynamic instability, described in Section II, the critical condition at which the instability occurs is not so obvious because the movement of the three-phase line is slow. This method also has the disadvantage that a cone surface must be prepared for each test in order to measure contact angles. On the other hand, it is easier to recognize the

Copyright n 2004 by Marcel Dekker, Inc. All Rights Reserved.

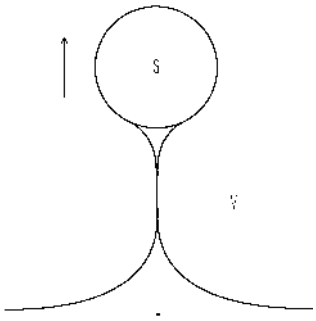

FIG. 36 Schematic of soap-like film when a solution of surface-active materials is used as the test liquid for the measurement using circular cylinder.

meniscus break-off in the method based on the geometrical instability discussed in Section III. In particular, the phenomenon can be seen more clearly when a circular cylinder is used as the test solid. However, when a solution of surface-active materials was used as the test liquid, a pair of two-dimensional menisci did not break under the critical condition shown in Fig. 23 since the liquid forms a thin soap-like film as shown in Fig. 36. The film maintains until it becomes a monolayer. Hence we cannot measure the contact angle by the method using a circular cylinder when the liquid includes surface-active materials. On the other hand, the meniscus formed under the inclined plate still breaks off even if surfactant solution is used since it contacts the wall of support S_2, as illustrated in Fig. 24. The method using a plate has another advantage in that it is possible to compensate the inaccuracy of the measurement near $\theta_R = 0^\circ$ or $\theta_A = 180^\circ$ if we use a support with a different inclination angle, as stated in Section III.B.

For the measurement of the liquid–vapor interfacial tension, we can use the three kinds of glass surfaces stated above, except when surfactant solution is used with a cylinder. The plate would be the most easily available among these surfaces. However, we must take care to clean the support or side plates shown in Figs. 24 and 32, as well as the glass plate, in order to not pollute the test liquid.

REFERENCES

1. Young, T. In *Miscellaneous Works*; Peacock, G., Ed.; J. Murray: London, 1855; Vol. 1, 418.
2. Chappius, J. In *Multiphase Science and Technology*; Hewitt, F., Delhaye, J.M., Zuber, N., Eds.; 1982; Vol. 1, 484.
3. Gaydos, J.; Neumann, A.W. In *Surfactant Science Series*; Neumann, A.W. Spelt, J.K., Eds.; Dekker: New York, 1996; Vol. 63, 169–238.

Copyright n 2004 by Marcel Dekker, Inc. All Rights Reserved.

4. Gibbs, J.W. *The Scientific Papers of J. Willard Gibbs*; Dover: New York, 1961; Vol. 1, 55–371.
5. Adamson, A.W. *Physical Chemistry of Surfaces,* 5th Ed.; John Wiley: New York, 1990.
6. Shuttleworth, R.; Bailey, G.L. Discuss. Faraday Soc. 1948, *3*, 16.
7. Johnson, R.E.; Dettre, R.H. Adv. Chem. Ser. 1964, *43*, 112.
8. Eick, J.D.; Good, R.J.; Neumann, A.W. J. Colloid Interface Sci. 1975, *53*, 235.
9. Hocking, L.M. J. Fluid Mech. 1976, *76*, 801.
10. Bayramli, E.; Mason, S.G. Can. J. Chem. 1981, *59*, 1962.
11. Cox, R.G. J. Fluid Mech. 1983, *131*, 1.
12. Joanny, J.F.; de Gennes, P.G. J. Chem. Phys. 1984, *81*, 552.
13. Jansons, K. J. Fluid Mech. 1985, *154*, 1.
14. Schwartz, L.W.; Garoff, S. J. Colloid Interface Sci. 1985, *106*, 422.
15. Chen, Y.L.; Helm, C.A.; Israelachvili, J.N. J. Phys. Chem. 1991, *95*, 10736.
16. Marmur, A. J. Colloid Interface Sci. 1994, *168*, 40.
17. Li, D.; Neumann, A.W. In *Surfactant Science Series*; Neumann, A.W. Spelt, J.K., Eds.; Dekker: New York, 1996; Vol. 63, 110–168.
18. Extrand, C.W. J. Colloid Interface Sci. 1998, *207*, 11.
19. Sakai, H.; Fujii, T. J. Colloid Interface Sci. 1999, *210*, 152.
20. Lam, C.N.C.; Wu, R.; Li, D.; Hair, M.L.; Neumann, A.W. Advances in Colloid and Interface Science, 2002, *96*, 169.
21. Kamusewitz, H.; Possart, W. Applied Physics A—Materials Science & Processing, 2003, *76*, 899.
22. Wilhelmy, L. Ann. Phys. 1863, *119*, 177.
23. Du Noüy, L. J. Gen. Physiol. 1919, *1*, 521.
24. Neumann, A.W.; Good, R.J. In *Surface and Colloid Science*; Good, R.J. Stromberg, R.R., Eds.; Plenum Press: New York, 1979; Vol. 22, 31–91.
25. Sugden, S. J. Chem. Soc. 1922, *121*, 858.
26. Harkins, W.D.; Brown, F.E. J. Am. Chem. Soc. 1919, *41*, 503.
27. Sugden, S. J. Chem. Soc. 1921, *120*, 1483.
28. de Laplace, P.S. *Mechanique Celeste, Supplement to Book 10*; J. B. M. Duprat: Paris, 1808.
29. Bashforth, F.; Adams, J.C. In *An Attempt to Test the Theory of Capillary Action*; University Press: Cambridge, 1883.
30. Andreas, J.M.; Hauser, E.A.; Tucker, W.B. J. Phys. Chem. 1938, *42*, 1001.
31. Hartland, S.; Hartley, R.W. In *Axisymmetric Fluid–Liquid Interfaces*; Elsevier: Amsterdam, 1976.
32. Fox, H.W.; Zisman, W.A. J. Colloid Sci. 1950, *5*, 520.
33. Adam, N.K.; Jessop, G. J. Chem. Soc. 1925, *1925*, 1863.
34. Bikerman, J.J. Ind. Eng. Chem. Anal. Ed. 1941, *13*, 443.
35. Paddy, J.F. In *Surface and Colloid Science*; Matijevic, E., Eirich, F.R., Eds.; Academic Press: New York, 1969; Vol, 1, 101–149.
36. Johnson, R.E.; Dettre, R.H. In *Surface and Colloid Science*; Matijevic, E., Eirich, F.R., Eds.; Academic Press: New York, 1969; Vol. 2, 85–153.
37. Ambwani, D.S.; Fort, T. In *Surface and Colloid Science*; Good, R.J., Stromberg, R.S., Eds.; Plenum Press: New York, 1979; Vol. 22, 93–119.

Copyright n 2004 by Marcel Dekker, Inc. All Rights Reserved.

38. Spelt, J.K.; Vargha-Butler, E.I. In *Surfactant Science Series*; Neumann, A.W., Spelt, J.K., Eds.; Dekker: New York, 1996; Vol. 63, 379–411.
39. Pallas, N.R. Colloids Surf. 1990, *43*, 169.
40. Suttiprasit, P.; Krisdhasima, V.; Mcguire, J. J. Colloid Interface Sci. 1992, *154*, 316.
41. Holcomb, C.D.; Zollweg, J.A. J. Colloid Interface Sci. 1992, *154*, 51.
42. Hasen, F.K. J. Colloid Interface Sci. 1993, *160*, 209.
43. Hong, K.T.; Imadojemu, H.; Webb, R.L. Exp. Therm. Fluid Sci. 1994, *8*, 279.
44. Lahooti, S.; Rio, O.I.D.; Neumann, A.W.; Cheng, P. In *Surfactant Science Series*; Neumann, A.W., Spelt, J.K., Eds.; Dekker: New York, 1996; Vol. 63, 441–507.
45. Song, B.; Springer, J. J. Colloid Interface Sci. 1996, *184*, 77.
46. Semmler, A.; Ferstl, R.; Kohler, H.H. Langmuir 1996, *12*, 4165.
47. Sedev, R.V.; Petrov, J.G.; Neumann, A.W. J. Colloid Interface Sci. 1996, *180*, 36.
48. Earnshaw, J.C.; Johnson, E.G.; Carrol, B.J.; Doyle, P.J. J. Colloid Interface Sci. 1996, *177*, 150.
49. Frank, B.; Garoff, S. Colloids Surf. 1999, *156*, 177.
50. Graham-Eagle, J.; Neumann, A.W. Colloids Surf. 2000, *161*, 63.
51. Sakai, K.; Mizuno, D.; Takagi, K. Physical Review E. 2001, *63*, Art No. 046302 Part 2.
52. Bateni, A.; Susnar, S.S.; Amirfazli, A.; Neumann, A.W. Colloids and Surfaces-Physicochemical and Engineering Aspects, 2003, *219*, 215.
53. Katoh, K.; Fujita, H.; Yamamoto, M. Trans. Jpn. Soc. Mech. Eng. 1991, *57(B)*, 4124. in Japanese.
54. Boruvka, L.; Gaydos, J.; Neumann, A.W. Colloids Surf. 1990, *43*, 307.
55. Ivanov, I.B.; Dimitrov, A.S.; Nikolov, A.D.; Denkov, N.D.; Kralchevsky, P.A. J. Colloid Interface Sci. 1992, *151*, 446.
56. Gu, Y.G. Colloids and Surfaces-Physicochemical and Engineering Aspects, 2001, *181*, 215.
57. Wenzel, R.N. Ind. Eng. Chem. 1936, *28*, 988.
58. Cassie, A.B.D. Discuss. Faraday Soc. 1948, *3*, 11.
59. Katoh, K.; Azuma, T. Heat Transf. Asian Res. 2001, *30*, 371.
60. Katoh, K.; Fujita, H.; Sasaki, H. Trans. ASME, J. Fluids Eng. 1995, *117*, 303.
61. Katoh, K.; Fujita, H.; Sasaki, H. Trans. ASME, J. Fluids Eng. 1990, *112*, 289.
62. Princen, H.M. In *Surface and Colloid Science*; Matijevic, E., Eirich, F.R., Eds.; Academic Press: New York, 1969; Vol. 2, 1–84.
63. Huh, C.; Scriven, L.E. J. Colloid Interface Sci. 1969, *30*, 323.
64. Rapacchietta, A.V.; Neumann, A.W. J. Colloid Interface Sci. 1977, *59*, 555.
65. Katoh, K.; Fujita, H.; Sasaki, H.; Miyashita, K. Trans ASME, J. Fluids Eng. 1992, *114*, 460.
66. Hirota, M.; Fujita, H.; Katoh, K. Proc. Third Int. Sympo. Multiphase Flow and Heat Transfer; Hemisphere: New York, 1994; 747.
67. Katoh, K.; Tsao, Y.; Yamamoto, M.; Azuma, T.; Fujita, H. J. Colloid Interface Sci. 1998, *202,*54.
68. Katoh, K.; Fujita, H.; Takaya, M. Trans. ASME, J. Fluids Eng. 1994, *116*, 801.

Copyright n 2004 by Marcel Dekker, Inc. All Rights Reserved.